 CMES, vol.54, no.2, pp.147-199, 2009

On the Location of Zeroes of Polynomials from the Stability Analysis of Novel Strong-Form Meshless Random Differential Quadrature Method

Hua Li[1], **Shantanu S. Mulay**[1] **and Simon See**[2]

Abstract: In this paper, the stability characteristics of a novel strong-form meshless method, called the random differential quadrature (RDQ), are studied using the location of zeros or roots of its characteristic polynomials with respect to unit circle in complex plane by discretizing the domain with the uniform or random field nodes. This is achieved by carrying out the RDQ method stability analysis for the 1^{st}-order wave, transient heat conduction and transverse beam deflection equations using both the analytical and numerical approaches. The RDQ method extends the applicability of the differential quadrature (DQ) method over irregular domain, discretized by randomly or uniformly distributed field nodes, by interpolating the function values based on the fixed reproducing kernel particle method (fixed RKPM). The stability analysis of the locally applied DQ and RDQ methods is carried out for the different single and multistep schemes by Von Neumann and Schur polynomials. The stable schemes are identified and their consistency analysis is carried out to obtain additional constraints on the temporal spacing. The analytical results from the stability and consistency analyses of the stable schemes are effectively verified by numerically implementing the RDQ method to solve the 1^{st}-order wave, transient heat conduction and transverse beam deflection equations by discretizing domain using uniform and random field nodes. Thus, it is shown that the RDQ method is very well attuned to the stability analysis and provides stable results as compared with FEM and other meshless methods.

Keywords: Meshless method, Von Neumann stability analysis, Schur polynomials, Random differential quadrature method, Differential quadrature.

[1] School of Mechanical and Aerospace Engineering, Nanyang Technological University, 50 Nanyang Avenue, Singapore 639798, Republic of Singapore

[2] Asia Pacific Science and Technology Center, Sun Microsystems, Inc., 1 Magazine Road, Singapore, 059567, Republic of Singapore

1 Introduction

The stability and consistency analyses of the numerical schemes have been one of the major topics of interest among the research community for a long time. For the schemes such as finite difference and finite element methods, lot of studies have been carried out in this area and well developed theories are available. As compared to these schemes, the differential quadrature (DQ) and smoothed particle hydrodynamics (SPH) are relatively new techniques.

The SPH method was proposed by Lucy (1977), and Gingold and Monaghan (1977) in which the function is approximated by its integral form using the window function. Balsara (1995) carried out Von Neumann (VN) stability analysis of the SPH method and suggested the optimal ranges of its parameters. He carried out the stability analysis by applying a constant velocity to an unperturbed state, verified the results using different kernels, and drawn conclusions based on the extensive numerical analyses. Borve, Omang and Trulsen (2004) applied the SPH method to solve the magnetohydrodynamics equations and carried out the stability analysis by small amplitude perturbations. Swegle, Hicks and Attaway (1995) obtained the SPH stability criterion in terms of the stress state because it was observed that when the SPH method is used with the cubic B-spline kernel, it gets unstable in the tensile region but remains stable in the compressive region. They explained that the instability is caused by a negative effective modulus resulting from the kernel function interaction with the constitutive equations. In other words, the instability is due to the effective stress, which amplifies rather than reduces the applied strain. Sigalotti and Lopez (2008) proposed an alternate method to reduce the tensile instability by an adaptive density kernel estimation algorithm such that the amount of smoothing applied to the data is controlled and the final smoothing length of the kernel is changed from point to point. Lisio, Grenier and Pulvirenti (1998) attempted the SPH method convergence for a generic polytropic fluid. A unified stability analysis was given by Belytschko, Guo, Liu and Xiao (2000) while addressing three types of instabilities namely the instability due to rank deficiency, tensile and the material instability. They applied the perturbation method to momentum equation and studied Eigenvalues of the resulting matrix. Fung (2002) used the DQ method to solve the 2^{nd}-order ordinary differential equation in time. He studied the stability and accuracy properties of the DQ method for the different grid point spacings. Tomasiello (2003) carried out the stability and accuracy analyses of the iterative based DQ method, called the iterative differential quadrature method. Aceto and Trigiante (2007) reviewed the stability properties results for linear multistep methods. Ata and Soulaimani (2005) used the SPH method to solve the shallow water equations and improved the dynamic stability of the method by introducing Lax-Friedrich scheme in it. Different approaches have been discussed in the past to impose the boundary conditions as the SPH method does not have a delta function property.

The MLPG method is a truly meshless method based on the local symmetric weak form that is applied over a local domain. Atluri and Shen (2002) discussed different global and local trial and test functions and provided a broad framework under which different MLPG forms can be derived by combining it with the different local trial and test functions. Atluri (2004), Atluri (2005), and Atluri and Shen (2002) in detail discussed the MLPG method with its application in the fluid and solid mechanics, respectively. Several MLPG mixed schemes are proposed like, finite difference method through MLPG [Atluri, Liu and Han (2006b)], MLPG mixed collocation method [Atluri, Liu and Han (2006a)], and finite volume method through MLPG [Atluri, Han and Rajendran (2004)]. These various MLPG mixed schemes are applied to solve a range of engineering analysis problems such as 3D contact problems [Han, Liu, Rajendran and Atluri (2006)], large deformation [Han, Rajendran and Atluri (2005)], crack analysis in the 2D and 3D domains [Sladek, Sladek, Zhang, Solek and Starek (2007)], heat conduction [XueHong, Shen and Tao (2007)], shell deformation [Jarak, Soric and Hoster (2007)], and thermo-piezoelectricity [Sladek, Sladek, Zhang and Solek (2007)]. Liu, Chen, Li and Cen (2008) developed a method for the structural dynamic problems, constructing the trial functions by the natural neighbour concept and using them with the general MLPG method. Cai and Zhu (2008) modified the original MLPG method to overcome Shepard partition of unity (PU) approximation drawbacks by employing a new PU based Shepard and least square interpolation approximation. Ma and Yan (2006) and Ma (2008) combined the MLPG method with the FEM and solved several problems [Ma (2007); Ma and Zhou (2009)]. Several researchers modified the MLPG method to solve the specific engineering problems such as limit analysis of plastic collapse [Chen, Liu and Cen (2008)], Navier-Stokes and energy equations [Arefmanesh, Najafi and Abdi (2008)], topology optimization [Li and Atluri (2008); Zheng, Long, Xiong and Li (2009)], microelectromechanical systems [Dang and Sankar (2008)], steady state and transient heat conduction analysis in the 3D solid [Sladek, Sladek, Tan and Atluri (2008)], elasto-plastic fracture analysis [Long, Liu and Li (2008)], thermal bending of Reissner-Mindlin plates [Sladek, Sladek, Solek and Wen (2008)], boundary and initial value problems in piezo-electric and magneto-electric-elastic solids [Sladek, Sladek, Solek and Atluri (2008)], 3D potential problems [Pini, Mazzia and Sartoretto (2008)], and freak wave generation [Ma (2007)].

The radial basis function (RBF) based collocation method was used to solve the Sturm-Liouville problem [Reutskiy (2008)], the modified equal width wave equation [Haq, Siraj and Ali (2008)], the nonlinear Schrodinger Equations [Haq, Siraj and Uddin (2009)], coupled heat transfer and fluid flow problem in Darcy porous media [Kosec and Šarler (2008)], and modeling of dynamic strain localization in quasi-brittle materials [Le, Mai-Duy, Tran-Cong and Baker (2008)]. Mai-Cao and Tran-Cong (2008) proposed a new meshless method, based on the level set method and semi-Lagrangian method coupled with the indirect RBF network method (IRBFNM), to capture the moving interfaces in passive transport problems; they also applied the IRBFNM to solve transient problems by combining it with different time integration schemes [Mai-Cao and Tran-Cong (2005)]. Young, Chen and Lee (2005) developed a method based on potential theory and desingularization technique and applied it to acoustic problems [Young, Chen and Lee (2006)]. Shaw, Banerjee and Roy (2008) developed a parametric modeling based meshless method, and Shaw and Roy (2007) developed a novel reproducing kernel interpolation method and applied it to nonlinear mechanics.

Bellman, Kashef and Casti (1972) proposed the DQ method by following the idea of an integral quadrature. As per it, the derivative at any point in a domain is approximated by the weighted sum of function values in whole domain provided that all domain points are collinear. They suggested two approaches, based on how the derivative term is approximated, to compute the weighting coefficients. The first approach uses the polynomial function as a test function and the second one uses a test function in which the coordinates of the grid points are chosen as the roots of the shifted Legendre polynomials. Both the approaches are not applicable for large order of algebraic system of equations due to highly ill-conditioned resulting matrix. To overcome it, Quan and Chang (1989a), and Quan and Chang (1989b) proposed another approach in which the weighting coefficients are computed by Lagrange interpolating polynomials. Shu, Khoo and Yeo (1994) proposed a so called general approach in which they combined both Bellman, and Quan and Chang approaches to compute the weighting coefficients. Liew, Zhang, Ng and Meguid (2003) applied the DQ method to model the elastic bonding in the 3D composite laminates. Shan, Shu and Lu (2008) coupled the local multiquadric-based RBF with the DQ method to solve the 3D curved boundary fluid flow problems. Liew, Huang and Reddy (2003) applied the MLS based DQ (MLSDQ) to solve the moderately thick plate for the shear deformation; they also applied the MLSDQ method to solve the 4^{th}-order thin plate bending differential equation over the irregular boundaries [Liew, Huang and Reddy (2004)].

The SPH method [Lucy (1977); Gingold and Monaghan (1977)] is not able to reproduce higher order terms well and does not satisfy the consistency condition. Liu, Jun and Zhang (1995) modified the SPH window function by introducing a correction function term and called it as the reproducing kernel particle method (RKPM). When this modified window function is fixed at a specific node, it is called the fixed RKPM. Wu, Chiu and Wang (2008) proposed a differential RKPM, in which separate differential reproducing condition sets were developed to compute the derivative shape functions instead of conventionally computing them by directly taking the RKPM approximation derivative. Wong and Shie (2008) carried out the large deformation analysis by the SPH based Galerkin method with the moving least square (MLS) approximation. Li, Liu and Wang (2008) used the RKPM method to carry out the ductile fracture simulations and shown that they are in well agreement with the existing experimental data and the finite element method (FEM).

The DQ method requires that all the field nodes should be aligned in a straight line in a collinear manner thus, the domain has to be regular. The main motivation behind the development of a novel strong-form meshless method called the RDQ method is to extend the applicability of the DQ method over an irregular domain discretized by uniformly or randomly distributed field nodes, which is shown by solving a plate with a hole problem by authors in Mulay, Li and See (2009), and Li, Mulay and See (2009). The quadrature nodes also called the virtual nodes are scattered in a domain and the governing equation is discretized at these virtual nodes. A function value at each virtual node is approximated by the surrounding field nodes using the fixed RKPM interpolation function. In order to avoid the DQ method getting unstable, as explained by Zong and Lam (2002), and Shu (2000), it is applied locally. A local DQ domain is created around each virtual node in the x and y directions, the virtual nodes falling in it are considered for a derivative discretization in the x and y directions, respectively, with respect to the central virtual node. The detailed convergence and consistency analyses of the RDQ method are carried out by the authors' [Mulay, Li and See (2009); Li, Mulay and See (2009)], and Mulay and Li (2009) applied the RDQ method to solve the microelectromechanical systems problems; the presented work is aimed at its elaborate stability analysis.

When a partial differential equation (PDE) contains the time and space derivative terms, the stable and consistent (without oscillations or dispersion in the solution) PDE discretization depends on how accurately the temporal marching is carried out. The time marching criterion can be determined by carrying out the numerical method stability analysis for the specific PDE. Hence, it is crucial for the numerical method to be attuned to carry out its stability analysis. It is shown in the presented work that the RDQ method can be used very well, to carry out the stability analysis and it provides the stable results with the domain discretized by either the uniform or random field nodes. This capability of the RDQ method makes it suitable to solve the complex problems involving the phenomenon such as moving boundaries, or the hydrogel swelling or de-swelling, in which the solution is highly sensitive to the time.

The motivation behind the presented work is to comprehensively study the stability characteristics of the RDQ method by the analytical and numerical approaches by discretizing the domain using the uniform as well as random field nodes. Most of the stability analysis works carried out in the past are based on either Eigen value analysis or the perturbation theory, or the numerical results based on the uniform field node spacing. In the presented novel approach, the stability analysis of the locally applied DQ and RDQ methods is demonstrated for several single and multi-step schemes of the temporal and spatial discretization based on Von Neumann and Schur polynomials as explained by Miller (1971) and Strikwerda (2004). For the 1^{st}-order wave equation, the stable schemes are identified and their consistency analysis is performed to identify additional constraints on the temporal spacing. The analytical results of these analyses are verified by numerically implementing the stable schemes using the RDQ method with the domain discretized by either the uniform or random field nodes. The stability analysis is further extended for the transient heat conduction and transverse beam deflection equations. For the transverse beam deflection problem, an analytical equation is developed to compute the successive deflection amplitude reductions for both the implicit and explicit approaches, and it is shown that the numerical amplitude reduction closely matches with the corresponding analytical values. It is also shown that an explicit approach by the RDQ method involves the dispersion effect thus $(v_2/v_1) > 1.0$ and $(v_2/v_1) \rightarrow 1.0$ as $k \rightarrow 0$ and the RDQ method implicit approach involves the dissipation effect thus $(v_2/v_1) < 1.0$ and $(v_2/v_1) \rightarrow 1.0$ as $k \rightarrow 0$, where k is the temporal spacing, ω_d is the damped natural frequency of the system, and let v_1 and v_2 be the reference field node deflection amplitudes with respect to the time t_1 and $(t_1 + 2\pi/\omega_d)$, respectively.

The objective of the presented work is to study the analytical and numerical stability characteristics of the locally applied DQ and RDQ methods in accordance with the VN and Schur polynomials and as applications, accurately solving the 1^{st}-order wave, transient heat conduction and the transverse beam deflection equations by the RDQ method coupled with the corresponding stability criteria with the domain discretized by either the uniform or random field nodes. For the complex PDE, it may not be possible to explicitly evaluate the stability criterion; this limitation is overcome by plotting the roots ϕ of the characteristic polynomial as $|\phi|^2$ versus (θ/π) and identifying the stability criterion from the plot. Thus, the presented work develops the broad framework, using which the transient PDEs' can be solved by carrying out their detailed stability analysis.

It is shown in the presented work that the RDQ method is very well attuned to carry out its stability analysis as compared with other existing meshless methods and the finite element method (FEM) as no mesh is involved thus, the RDQ method can be effectively used in the time dependent problems (linear and nonlinear) such as hydrogel swelling and crack propagation.

The outline of the paper is as follows. The RDQ method formulation is presented in Section 2. In Section 3, the VN and Schur polynomials are explained and detailed stability analysis using the 1^{st}-order wave equation is carried out; the stable schemes are identified and their elaborate consistency analysis is performed to obtained additional constraints on the temporal spacing. In Section 4, the stability analysis is further extended to solve the transient heat conduction equation using the RDQ method with the domain discretized by either the uniform or random field nodes. In Section 5, the transverse beam deflection equation is solved by the RDQ method using both the implicit and explicit approaches, and the numerical deflection amplitude reduction is compared with the corresponding analytical values, the conclusions are given in Section 6.

2 Random differential quadrature method

In the RDQ method, the governing differential equation is discretized in a strong form at virtual nodes by applying the DQ method locally, and the function values at each virtual node are interpolated by surrounding field nodes through the fixed RKPM interpolation function.

2.1 Fixed RKPM interpolation function

The fixed RKPM interpolation function was developed from the SPH method [Lucy (1977)] by modifying its kernel [Liu, Jun, and Zhang (1995)]. Even though it does not have a delta function property $\left[f_I \neq f^h(x,y)_I\right]$, it has several advantages like a partition of unity, constant moment matrix and less computation efforts. The function value approximation as per the fixed RKPM interpolation is given by,

$$f^h(x,y) = \int\limits_{\Omega} C(x,y,u,v)K(x_k-u,y_k-v)f(u,v)dudv \tag{1}$$

where $f^h(x,y)$ is a function approximation of the function $f(x,y)$ at a virtual node (x,y), and $K(x_k-u,y_k-v)$ is a kernel function fixed at the virtual node (x_k,y_k). The unknown correction functions, $C(x,y,u,v) = B^T(u,v)c(x,y)$, where, $B^T(u,v)_{(m\times 1)} = \left\{b_1(u,v),\quad b_2(u,v),\quad \ldots,\quad b_m(u,v)\right\}$ is a $m-$order column vector of the monomials, are determined by the consistency or reproducing condition. After simplifying, the shape functions are given as,

$$f^h(x,y) = \sum_{I=1}^{NP} N_I(x,y)u_I, \text{ where } I=1 \text{ to } NP \text{ are interpolation nodes} \tag{2}$$

where, $N_I(x,y)$ and u_I are the fixed RKPM shape function and the field nodal parameters, respectively [Aluru (2000); Aluru and Li (2001)]. The kernel function K is constructed by correctly reproducing the window function w as,

$$K(x_k-u, y_k-v) = \frac{1}{d_x} w\left(\frac{x_k-u}{d_x}\right) \frac{1}{d_y} w\left(\frac{y_k-v}{d_y}\right) \tag{3}$$

where d_x and d_y are cloud sizes in the x and y directions, respectively. Eq. (3) shows that the kernel function, K, is represented in the window function form, w. In the RDQ method, a cubic spline function is used as the window function,

$$w(z_I) = \begin{cases} 0, & z_I < -2 \\ \frac{1}{6}(z_I+2)^3, & -2 \le z_I \le -1 \\ \frac{2}{3} - z_I^2(1+\frac{z_I}{2}), & -1 \le z_I \le 0 \\ \frac{2}{3} - z_I^2(1-\frac{z_I}{2}), & 0 \le z_I \le 1 \\ \frac{-1}{6}(z_I-2)^3, & 1 \le z_I \le 2 \\ 0, & z_I > 2 \end{cases} \tag{4}$$

It is seen from Eq. (4) that the window function is nonzero over a sub-domain $[-2,2]$ and zero outside of it. The window function integral over the sub-domain $[-2,2]$ is one, namely it has c^0consistency. Due to this property, the summation of field node shape function values, which are used for the function value interpolation, is equal to one as given below.

$$\sum_{I=1}^{NP} N_I(x,y) = 1 \tag{5}$$

Atluri and Shen (2002), and Jin, Li and Aluru (2001) discussed the RKPM and MLS shape functions equivalence. Atluri and Shen (2002) shown that if the same kernel and the window functions are chosen in the RKPM and MLS, respectively, with the same consistency order, k, the resulting shape functions are identical.

2.2 Differential quadrature formulation

In the DQ method, a derivative term is approximated by assuming different test or approximation functions [Bellman, Kashef and Casti (1972); Quan, and Chang (1989a); Quan, and Chang (1989b); Shu (2000)]. In the RDQ method, Shu's general approach [Shu (2000)] based on Lagrange interpolation as a test function is adopted. For N_x grid points, $x_1, x_2, ..., x_{N_x}$, in a domain, the 1^{st}-order derivative

$f^{(1)}(x)$ of a function $f(x)$ with sufficiently smooth property at any field node is approximated by,

$$f_{,x}^{(1)}(x_i) = \sum_{j=1}^{N_x} a_{ij} f(x_j), \text{ for } i = 1, 2, ..., N_x \tag{6}$$

where $f_x^{(1)}(x_i)$ is an approximate 1^{st}-order derivative of $f(x)$ at x_i and a_{ij} are the DQ weighting coefficients. For the 2-D problem, $f(x,y)$ derivatives are discretized as,

$$f_{,x}^{(1)}(x_i, y_j) = \sum_{k=1}^{N_x} a_{ik}^x f(x_k, y_j), \text{ for } i = 1, 2, ..., N_x \tag{7}$$

$$f_{,y}^{(1)}(x_i, y_j) = \sum_{k=1}^{N_y} a_{jk}^y f(x_i, y_k), \text{ for } j = 1, 2, ..., N_y \tag{8}$$

where, a_{ik}^x and a_{jk}^y are the $f_x^{(1)}(x_i, y_j)$ and $f_y^{(1)}(x_i, y_j)$ DQ weighting coefficients, respectively, N_x and N_y are the total virtual nodes located inside the DQ local domain in the x and y directions, respectively. Once the weighting coefficients a_{ik}^x and a_{jk}^y are determined, the numerical bridge to link the discretized derivative terms from the governing differential equation with the field node function values approximation is established through the fixed RKPM function. In the RDQ method, the weighting coefficients are calculated by Shu's general approach [Shu (2000)] as given in Eqns. (9) to (13) below,

$$a_{ik}^x = \frac{1}{x_i - x_k} \prod_{m=1, m\neq i,k}^{N_x} \left(\frac{x_i - x_m}{x_k - x_m} \right) \text{ and } a_{ii}^x = -\sum_{k=1_{k\neq i}}^{N_x} a_{ik}^x \tag{9}$$

Similar expressions can be written for the weighting coefficients a_{ik}^y and a_{ii}^y which are used in the 1^{st}-order derivative DQ discretization with respect to the y direction.

$$a_{ik}^y = \frac{1}{y_i - y_k} \prod_{\substack{m=1 \\ m\neq i,k}}^{N_y} \left(\frac{y_i - y_m}{y_k - y_m} \right) \text{ and } a_{ii}^y = -\sum_{k=1_{k\neq i}}^{N_y} a_{ik}^y \tag{10}$$

The 2^{nd}-order derivative discretization for the 1-D case is given as,

$$f_{,x}^{(2)}(x_i) = \sum_{j=1}^{N_x} b_{ij} f(x_j) \tag{11}$$

$$b_{ij} = 2a_{ij}\left[a_{ii} - \frac{1}{x_i - x_j}\right] \text{ for } i,j = 1,2,\ldots,N_x \quad i \neq j \tag{12}$$

$$b_{ii} = -\sum_{j=1_{j\neq i}}^{N_x} b_{ij} \text{ for } i = 1,2,\ldots,N_x \tag{13}$$

Similar expressions can be written for the 2-D case as well as given by Shu [Shu (2000)].

2.3 The RDQ method

In the RDQ method [Mulay, Li and See (2009)], the cosine or uniformly distributed background nodes, called the virtual nodes, are created as shown in Fig. 1. The field nodes are scattered in a uniform or random manner. A local domain is created around each virtual node as shown in Fig. 1, the field nodes falling in it are taken into consideration for the virtual node function value approximation. The local DQ domain is created around each virtual node in the x and y directions, the virtual nodes falling in it are taken into consideration for the governing equation discretization at that virtual node by locally applying the DQ method.

The governing equation is discretized at all internal domain virtual nodes, the virtual node function value expressions from the DQ derivative discretization equations are replaced by the virtual node function values approximation equations obtained by the fixed RKPM interpolation function.

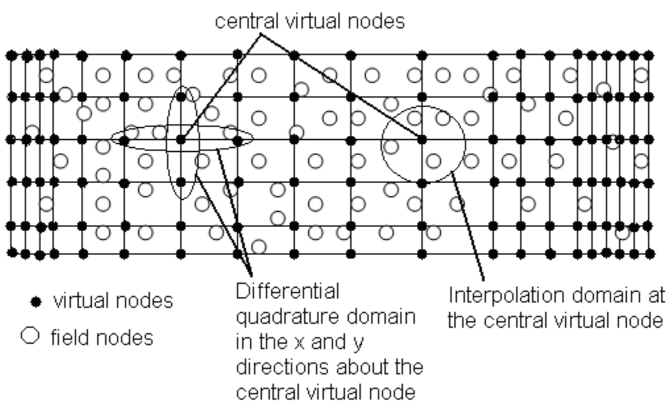

Figure 1: Local function value interpolation and the DQ domain creation in the RDQ method.

In this way, the governing equation discretization at the virtual nodes is represented in the field nodes unknown nodal parameter values algebraic form. The boundary conditions are also imposed in the strong form. Let's consider Eq. (11) as one of the derivative terms in the governing PDE, it is expanded by locally applying the DQ method as,

$$\frac{d^2 f(x_i, y_j)}{dx^2} = \begin{Bmatrix} b_{i1} & b_{i2} & \cdots & b_{iN_x} \end{Bmatrix}_{1\times N_x} \begin{bmatrix} f^h(x_1, y_j) \\ f^h(x_2, y_j) \\ \vdots \\ f^h(x_{N_x}, y_j) \end{bmatrix}_{N_x \times 1} \tag{14}$$

The virtual node function value approximation terms from Eq. (14) are replaced by the fixed RKPM interpolation equations expressed by Eq. (2),

$$\frac{d^2 f(x_i, y_j)}{dx^2} = \begin{Bmatrix} b_{i1} & \cdots & b_{iN_x} \end{Bmatrix}_{1\times N_x} \begin{bmatrix} N_1(x_1, y_j) & \cdots & N_{NP}(x_1, y_j) \\ \vdots & \ddots & \vdots \\ N_1(x_{N_x}, y_j) & \cdots & N_{NP}(x_{N_x}, y_j) \end{bmatrix}_{(N_x \times NP)} \begin{bmatrix} u_1 \\ u_2 \\ \vdots \\ u_{NP} \end{bmatrix}_{(NP\times 1)} \tag{15}$$

In this way, the derivative terms from the governing differential equation are represented in the form of field nodes unknown nodal parameters. For detailed RDQ method, please refer Mulay, Li and See (2009), and Li, Mulay and See (2009).

3 The RDQ method stability analysis by 1^{st}-order wave equation

As well known, it is essential to understand the numerical methods stability and consistency behaviours to ensure it to converge. The detailed consistency analysis of the RDQ method is carried out by authors' in [Mulay, Li and See (2009)] and in this section, its stability analysis is performed for the 1^{st}-order wave equation, $\phi_{,t} = a\phi_{,x}$, by several single and multi-step schemes. The single-step schemes are studied by Von Neumann stability analysis [Strikwerda (2004)] and the multi-step schemes by Schur and Neumann polynomials [Miller (1971); Strikwerda (2004)].

The VN and Schur polynomials appear frequently in the PDE studies. Let a general polynomial be represented as $\phi(z) = \sum_{l=0}^{d} a_l z^l$, where d is the polynomial order and a_l are its coefficients. The polynomial $\phi(z)$ is called as Schur polynomial if its all roots are located within the unit radius circle i.e. $|\phi_i| < 1.0$, where $i = 1, 2, ..., d$. The polynomial $\phi(z)$ is called as the VN polynomial if some of the roots are located within the unit circle and the remaining are on the circle but none is outside of it i.e. $|\phi_i| \leq 1.0$, where $i = 1, 2, ..., d$.

In the Neumann analysis, after the wave equation is discretized, its amplification factor, $g(h\xi)$, is derived by taking the inverse Fourier transform and simplifying it to give $\hat{\upsilon}_n(\xi) = g(h\xi)\,\hat{\upsilon}_0(\xi)$ where, h is the spatial spacing, $\xi \subset [-\pi, \pi]$ is Fourier domain, and $\hat{\upsilon}_n$ and $\hat{\upsilon}_0$ are the n^{th} and 0^{th} time level function values, respectively [Strikwerda (2004)]. The amplification factor, $g(h\xi)$, is analyzed for the stability criterion. In Schur and Neumann polynomial analyses, the amplification or characteristic polynomial is derived by discretizing the wave equation, the roots of this polynomial are examined to classify the polynomial as either Schur, $P(n,0,0)$, or VN polynomial [Miller (1971)], $P(k, n-k, 0)$, where n are the total polynomial roots out of which k roots lie within unit circle on the complex plane.

3.1 The 1^{st}-order wave equation stability analysis using different schemes

In this section, different time and the space discretization schemes are studied for the stability by the 1^{st}-order wave equation, and the stable schemes are identified.

3.1.1 Central time and central space with multi-step

In this scheme, three virtual nodes are considered in the time and space domains stencil, respectively, as shown in Fig. 2.

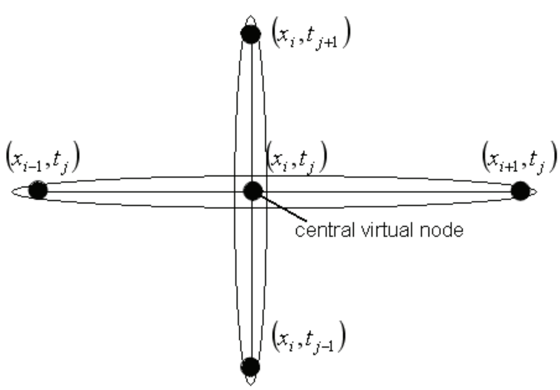

Figure 2: Local DQ domain around a virtual node inside computational domain.

The 1^{st}-order wave equation, $\phi_{,t} = a\phi_{,x}$, in the discretized form is given as,

$$\Rightarrow \left\{ a_{j,j-1} \quad a_{j,j} \quad a_{j,j+1} \right\} \begin{Bmatrix} \phi(x_i, t_{j-1}) \\ \phi(x_i, t_j) \\ \phi(x_i, t_{j+1}) \end{Bmatrix} = a \left\{ a_{i,i-1} \quad a_{i,i} \quad a_{i,i+1} \right\} \begin{Bmatrix} \phi(x_{i-1}, t_j) \\ \phi(x_i, t_j) \\ \phi(x_{i+1}, t_j) \end{Bmatrix} \tag{16}$$

The weighting coefficients in Eq. (16) are computed as per Eqns. (9) and (10). The inverse Fourier transform is employed in the resulting equation to get a characteristic polynomial as (please refer Appendix A),

$$\phi(z) = z^2 - (2ri\sin\theta)z - 1 \tag{17}$$

where, $r = (at/h)$ is Courant number. By comparing Eq. (17) with the generalized polynomial given in Eq. (18), its coefficients are given in Eq. (19),

$$\phi(z) = \sum_{l=0}^{d} a_l z^l \tag{18}$$

$$a_0 = -1, \quad a_1 = 2ri\sin\theta, \quad a_2 = 1 \tag{19}$$

where, d is the polynomial order. The complex conjugate polynomial of Eq. (17) is given in Eq. (21) using Eq. (20),

$$\phi^*(z) = \sum_{l=0}^{d} \overline{a}_{d-l} z^l \tag{20}$$

$$\phi^*(z) = 1 + (2ri\sin\theta)z - z^2 \tag{21}$$

As such,

$$|\phi^*(0)| = 1 \text{ and } |\phi(0)| = 1 \text{ so } \phi_1(z) = \frac{\phi_0^*(0)\phi(z) - \phi(0)\phi_0^*(z)}{z} = 0 \tag{22}$$

where, $\phi_1(z)$ is a reduced polynomial (Please refer Appendix B). As $\phi_1(z) = 0$, $\phi(z)$ is a self-inversive polynomial [Miller (1971)]. As per the theorem given by Miller (1971), a self-inversive polynomial $\phi(z)$ is the VN polynomial if $\phi^{(1)}(z)$ is the VN polynomial, where $\phi^{(1)}(z)$ is a 1^{st}-order $\phi(z)$ derivative. Therefore, using Eq. (17), its 1^{st}-order derivative is written as,

$$g(z) = \phi^{(1)}(z) = 2z - 2ri\sin\theta \tag{23}$$

The complex conjugate polynomial of Eq. (23) is given as,

$$g^*(z) = 2 + 2ri\sin\theta z \tag{24}$$

from Eqns. (23) and (24), $|g^*(0)| = 2$ and $|g(0)| = 2ri\sin\theta$. For Eq. (23) being the VN polynomial, $|g^*(0)|^2 - |g(0)|^2 \geq 0$. This condition results in,

$$|r| \leq 1 \tag{25}$$

this indicates that Eq. (23) is the VN polynomial only if Eq. (25) is satisfied, then Eq. (17) becomes the VN polynomial. Thus, Eq. (25) is the stability condition for this scheme. The forward time (two nodes) and central space (three nodes) scheme can be used as an initialization scheme. The initialization scheme does not affect the multi-step schemes stability as the amplification factor is controlled by the stability criterion so, even if there is any solution instability due to initialization scheme, it does not propagate with time.

3.1.2 Central time and forward space with multi-step.

In this scheme, three virtual nodes are considered in the time and space domains, respectively, as shown in Fig. 3.

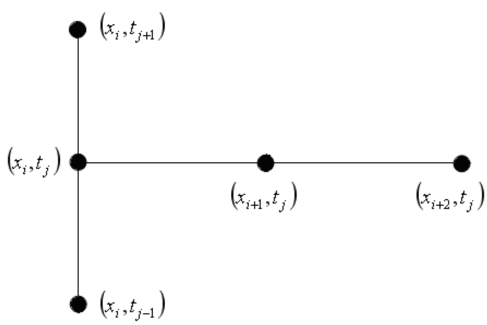

Figure 3: Central time and forward space scheme of domain discretizations for the 1^{st}-order wave equation.

The 1^{st}-order wave equation in the discretized form is given as,

$$\phi_{,t} = a\phi_{,x} \Rightarrow$$

$$\left\{a_{j,j-1} \quad a_{j,j} \quad a_{j,j+1}\right\} \begin{Bmatrix} \phi(x_i, t_{j-1}) \\ \phi(x_i, t_j) \\ \phi(x_i, t_{j+1}) \end{Bmatrix} = a\left\{a_{i,i} \quad a_{i,i+1} \quad a_{i,i+2}\right\} \begin{Bmatrix} \phi(x_i, t_j) \\ \phi(x_{i+1}, t_j) \\ \phi(x_{i+2}, t_j) \end{Bmatrix} \tag{26}$$

The weighting coefficients are computed by Eqns. (9) and (10). The characteristic polynomial is derived by applying the inverse Fourier transform to obtain [Miller (1971)] (Please refer Appendix A),

$$\phi(z) = z^2 + (\alpha + i\beta)z - 1 \tag{27}$$

where $\gamma = \cos\theta - 2$, $\alpha = 2r[1 + \cos\theta\gamma]$, $\beta = 2r\sin\theta\gamma$. By comparing Eq. (27) with Eq. (18), its coefficients are given as,

$$a_0 = -1, \quad a_1 = \alpha + i\beta, \quad a_2 = 1 \tag{28}$$

The complex conjugate polynomial of Eq. (27) is given as,

$$\phi^*(z) = 1 + (\alpha - i\beta)z - z^2 \tag{29}$$

from Eqns. (27) and (29),

$$|\phi^*(0)| = 1 \text{ and } |\phi(0)| = 1, \text{ so } \phi_1(z) = 0 \tag{30}$$

where, $\phi_1(z)$ is a reduced polynomial (Please refer Appendix B). As $\phi_1(z) = 0$, $\phi(z)$ is a self-inversive polynomial. Eq. (27) is the VN polynomial only if $\phi^{(1)}(z)$ is the VN polynomial [Miller (1971)], where $\phi^{(1)}(z)$ is the 1^{st}-order $\phi(z)$ derivative. From Eq. (27),

$$g(z) = \phi^{(1)}(z) = 2z + (\alpha + i\beta) \tag{31}$$

$$g^*(z) = 2 + (\alpha - i\beta)z \tag{32}$$

From Eqns. (31) and (32), $|g^*(0)| = 2$ and $|g(0)| = \alpha + i\beta$. For Eq. (32) being the VN polynomial, $|g^*(0)|^2 - |g(0)|^2 \geq 0$. This condition results in,

$$r^2\left[1 + \gamma^2 + 2\gamma\cos\theta\right] \leq 1 \tag{33}$$

in which, $\left|1 + \gamma^2 + 2\gamma\cos\theta\right| \leq 1$ for $|r| \leq 1$. Maximum of $(1 + \gamma^2 + 2\gamma\cos\theta)$ is at $\cos\theta = 4/3$ which gives,

$$|r| \leq 3i \tag{34}$$

Eq. (34) is the stability condition for this scheme. It is seen that this is a complex number but it's impossible to have a complex number as the stability criterion. Thus $g(z)$ is not the VN polynomial and hence, $\phi(z)$ is also not the VN polynomial, as a result, this scheme is unstable. Let ϕ_+ and ϕ_- be the roots of Eq. (27), a graph of $|\phi_+|^2$ versus θ/π is plotted and ϕ_+ is found to be unconditionally stable, and a graph of $|\phi_-|^2$ versus θ/π is plotted and ϕ_- is found to be unstable as shown in Figs. 4a and 4b by $0 \leq r \leq 2$ and $0 \leq r \leq 1$, respectively.

3.1.3 Forward time and forward space with multi-step

In this scheme, three virtual nodes are considered in the time and space domain stencils, respectively, as shown in Fig. 5.

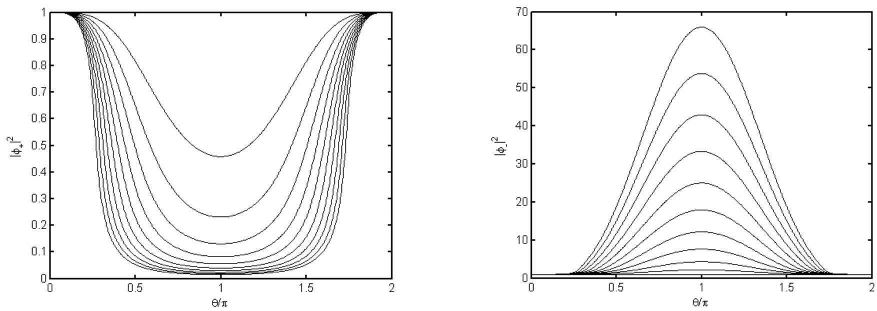

a **b**

Figure 4: a) $|\phi_+|^2$ versus θ/π plot by numerically implementing the 2^{nd} stability scheme with r from 0 to 2, b) $|\phi_-|^2$ versus θ/π plot by numerically implementing the 2^{nd} stability scheme with r from 0 to 1.

The 1^{st}-order wave equation, $\phi_{,t} = a\phi_{,x}$, in the discretized form is given as,

$$\Rightarrow \left\{ a_{j,j} \quad a_{j,j+1} \quad a_{j,j+2} \right\} \left\{ \begin{matrix} \phi(x_i,t_j) \\ \phi(x_i,t_{j+1}) \\ \phi(x_i,t_{j+2}) \end{matrix} \right\} = a \left\{ a_{i,i} \quad a_{i,i+1} \quad a_{i,i+2} \right\} \left\{ \begin{matrix} \phi(x_i,t_j) \\ \phi(x_{i+1},t_j) \\ \phi(x_{i+2},t_j) \end{matrix} \right\} \tag{35}$$

The weighting coefficients from Eq. (35) are computed by Eqns. (9) and (10), and its characteristic polynomial is given as (Please refer Appendix A),

$$\phi(z) = z^2 - 4z + 3 - (\alpha + i\beta) \tag{36}$$

where $\gamma = \cos\theta - 2$, $\alpha = 2r[1 + \cos\theta\gamma]$, $\beta = 2r\sin\theta\gamma$. The complex conjugate polynomial of Eq. (36) is given as,

$$\phi^*(z) = 1 - 4z + (3 - \alpha + i\beta)z^2 \tag{37}$$

from Eqns. (36) and (37), $|\phi^*(0)| = 1$ and $|\phi(0)| = 3 - \alpha - i\beta$. For Eq. (36) to be VN polynomial, $|\phi^*(0)|^2 - |\phi(0)|^2 \geq 0$ [Miller (1971)] hence,

$$1 - (3 - \alpha)^2 - \beta^2 \geq 0 \tag{38}$$

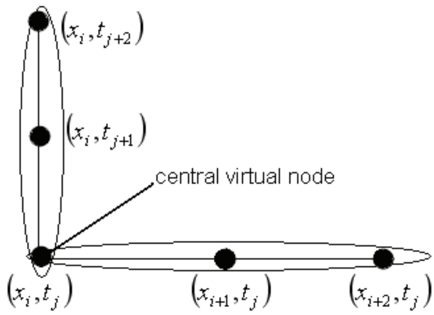

Figure 5: Multi-step scheme of forward time and space domain discretizations for the 1^{st}-order wave equation.

It is difficult to analytically solve Eq. (38) thus, the roots of $\phi(z)$ are studied by plotting the graph of $|\phi|^2$ versus θ/π by incrementing r from 0 to 1 and angle from 0 to 2π. The graph of $|\phi_+|^2$ versus θ/π shows that $|\phi_+|^2$ has the lowest magnitude of 9, as shown in Fig. 6a. The graph of $|\phi_-|^2$ versus θ/π shows that $|\phi_-|^2$ is stable for $|r| \leq 1$, as shown in Fig. 6b. This scheme is unstable because of the $|\phi_+|$ instability.

3.1.4 Forward time and forward space with single step

In this scheme, two and three virtual nodes are used in the time and space domains respectively, as shown in Fig. 7. The 1^{st}-order wave equation in the discretized form is given as,

$$\phi_{,t} = a\phi_{,x} \Rightarrow \begin{Bmatrix} a_{j,j} & a_{j,j+1} \end{Bmatrix} \begin{Bmatrix} \phi(x_i, t_j) \\ \phi(x_i, t_{j+1}) \end{Bmatrix} = a \begin{Bmatrix} a_{i,i} & a_{i,i+1} & a_{i,i+2} \end{Bmatrix} \begin{Bmatrix} \phi(x_i, t_j) \\ \phi(x_{i+1}, t_j) \\ \phi(x_{i+2}, t_j) \end{Bmatrix} \tag{39}$$

The characteristic polynomial of Eq. (39) is given as (Please refer Appendix A),

$$\phi(z) = z - (1 + \alpha + i\beta) \tag{40}$$

where $\gamma = 2 - \cos\theta$, $\alpha = r[-1 + \cos\theta\gamma]$, $\beta = r\sin\theta\gamma$. The complex conjugate polynomial of Eq. (40) is given as,

$$\phi^*(z) = -(1 + \alpha - i\beta)z + 1 \tag{41}$$

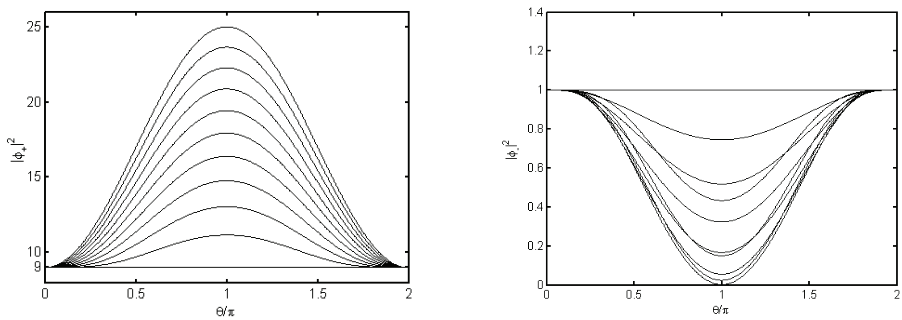

a **b**

Figure 6: By numerically implementing the multi-step forward time and space scheme with r from 0 to 1 a) $|\phi_+|^2$ versus θ/π plot shows the constant magnitude of 9, which means that this root is located outside the unit circle, b) $|\phi_-|^2$ versus θ/π plot shows that the root is located inside the unit circle.

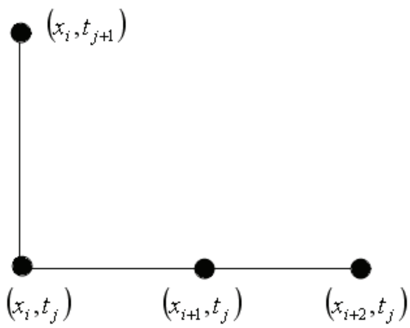

Figure 7: Single-step scheme of forward time and space domain discretizations for the 1^{st}-order wave equation.

By Eqns. (40) and (41), $|\phi^*(0)| = 1$, $|\phi(0)| = -(1+\alpha+i\beta)$. For Eq. (40) to be a VN polynomial $|\phi^*(0)\,|^2 - |\phi(0)\,|^2 \geq 0$,

$$1 - \left[(1+\alpha)^2 + \beta^2\right] \geq 0 \tag{42}$$

Simplifying Eq. (42) results in,

$$|r| \leq \frac{2}{7} \text{ and } |r| > 0 \tag{43}$$

Eq. (43) is the stability condition for this scheme. The plot of $|\phi|^2$ versus θ/π by incrementing the r from 0 to 1 and angle from 0 to 2π also shows that the scheme is stable for $|r| \leq 0.2$, which is very close to Eq. (43), as shown in Fig. 8. This scheme is nothing but an upwind technique as the wave in $\phi_{,t} = a\phi_{,x}$ is traveling towards the left.

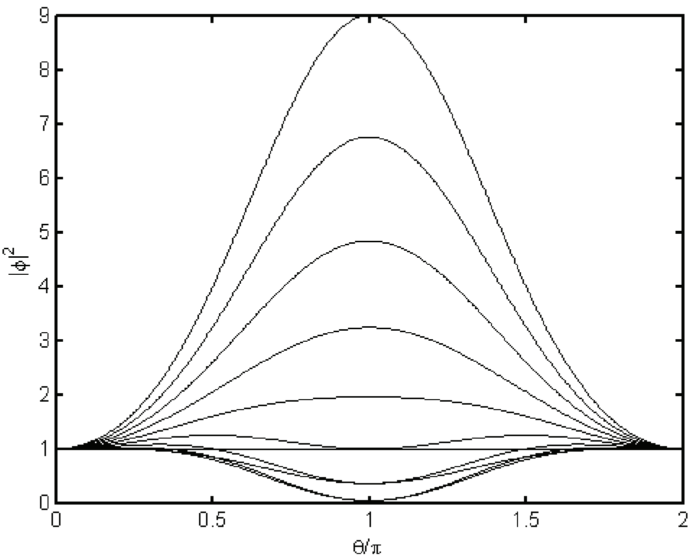

Figure 8: $|\phi|^2$ versus θ/π plot for the single-step forward time and space scheme with r from 0 to 1. It shows that the root is inside of the unit circle for $|r| \leq 0.2$.

3.1.5 Forward time and central space with single step

In this scheme, two and three virtual nodes are used in the time and space domains, respectively, as shown in Fig. 9. The 1^{st}-order wave equation in the discretized form is given as,

$$\phi_{,t} = a\phi_{,x} \Rightarrow \left\{ a_{j,j} \quad a_{j,j+1} \right\} \left\{ \begin{matrix} \phi(x_i, t_j) \\ \phi(x_i, t_{j+1}) \end{matrix} \right\} = a \left\{ a_{i,i-1} \quad a_{i,i} \quad a_{i,i+1} \right\} \left\{ \begin{matrix} \phi(x_{i-1}, t_j) \\ \phi(x_i, t_j) \\ \phi(x_{i+1}, t_j) \end{matrix} \right\} \tag{44}$$

The amplification factor of Eq. (44) is given in Eq. (46) as,

$$g^{n+1} = \left\{ \frac{r}{2} \left[2i \sin\theta \right] + 1 \right\} g^n \tag{45}$$

$$g(\theta) = 1 + ir\sin\theta \tag{46}$$

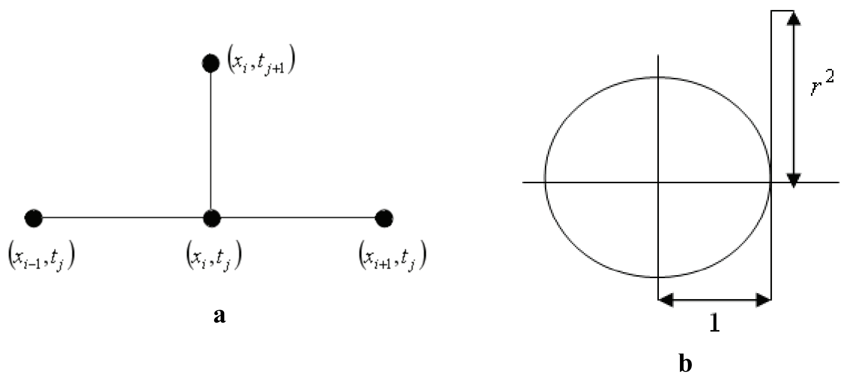

Figure 9: a) Single-step forward time and central space domains discretization for the 1^{st}-order wave equation, b) The amplification factor plot in the complex plane. It is seen that the scheme is unstable.

When Eq. (46) is plotted in the complex plane, as shown in Fig. 9b, it's found to be unstable. If $\phi^m = \left(\phi^n_{m-1} + \phi^n_{m+1}\right)/2$ is substituted in Eq. (44), similar to Lax-Friedrich scheme in the finite difference, it is rewritten as,

$$\phi^{n+1}_m = \frac{r}{2}\left[\phi^n_{m+1} - \phi^n_{m-1}\right] + \left[\frac{\phi^n_{m-1} + \phi^n_{m+1}}{2}\right] \tag{47}$$

The new amplification factor from Eq. (47) is given as,

$$g(\theta) = \cos\theta + ir\sin\theta, \quad \therefore |g(\theta)| \Rightarrow |r| \leq 1 \tag{48}$$

in which, it is clear that for $|r| \leq 1$, the scheme is stable.

3.2 Consistency analysis of the stable schemes and their verification by numerically implementing the 1st-order wave equation by the locally applied DQ method

It is essential to ensure that the constraints on r obtained from the stability analysis should not contradict with that of the obtained from consistency analysis. To fulfill this requirement, the consistency analysis of the stable schemes, which are obtained in the previous section, is carried out. The stable schemes are numerically implemented to solve the 1^{st}-order wave equation, with $\phi\left(x,0\right) = \sin\left(2\pi x\right)$

and $\phi\,(0,t) = \phi\,(1,t) = 0$ when $x \in [0,1]$ as the initial and periodic boundary conditions, respectively.

Let a PDE in its continuous and discretized form be given as $Pu = f$ and $P(h_x, h_y)u = f$, respectively, where $h_x = L_x/(NP_x - 1)$ and $h_y = L_y/(NP_y - 1)$ are the nodal spacings, L_x and L_y are the domain lengths, and NP_x and NP_y are the total number of field nodes in the x and y directions, respectively. The numerical discretization scheme is called as consistent if the PDE in its discretized form closely approximates the corresponding continuous form as h_x and $h_y \to 0$ i.e. $Pu - P(h_x, h_y)u \to 0$, as $h_x, h_y \to 0$ so that there is no numerical discretization error involved in the simulation.

The discretization equation for the central time and space scheme (Scheme 1) given in Eq. (16) is obtained by Taylor series expansion [Mulay, Li and See (2009)], and written as (Please refer Appendix C),

$$\phi_{,t} - a\phi_{,x} = \phi_{,xxx}\left[\frac{ah^2}{6} - \frac{t^2a^3}{6}\right] \tag{49}$$

This scheme is consistent as $\phi_{,t} - a\phi_{,x} \to 0,$ as h and $t \to 0$. Eq. (49) is the numerically solved exact wave equation. As $\phi_{,xxx}$ is the dispersion with respect to space domain, it is desirable to have a negative or zero value for it thus,

$$\left[\frac{ah^2}{6} - \frac{t^2a^3}{6}\right] \leq 0 \tag{50}$$

simplifying Eq. (50) gives,

$$|r| \geq 1 \tag{51}$$

It is observed from Eq. (51) that the consistency condition is same as the stability condition as given in Eq. (25) for $|r| = 1$. This scheme is numerically implemented to solve the 1^{st}-order wave equation. When $r = 1$, the wave is preserved for the total time and no instability is observed as shown in Fig. 10a. When $r = 0.5$, still the initial wave is preserved throughout the time and no dissipation is observed as shown in Fig. 10b; this is expected as no dissipation term is present in Eq. (49). For $r = 2$ however, the instability is observed, as shown in Fig. 10c, due to the stability condition violation.

For the forward time and space scheme (scheme 4) given in Eq. (39), the discretization equation using Taylor series expansion [Mulay, Li and See (2009)], is written as (Please refer Appendix C),

$$\phi_{,t} - a\phi_{,x} = \phi_{,xx}\left[\frac{-ahr}{2}\right] \tag{52}$$

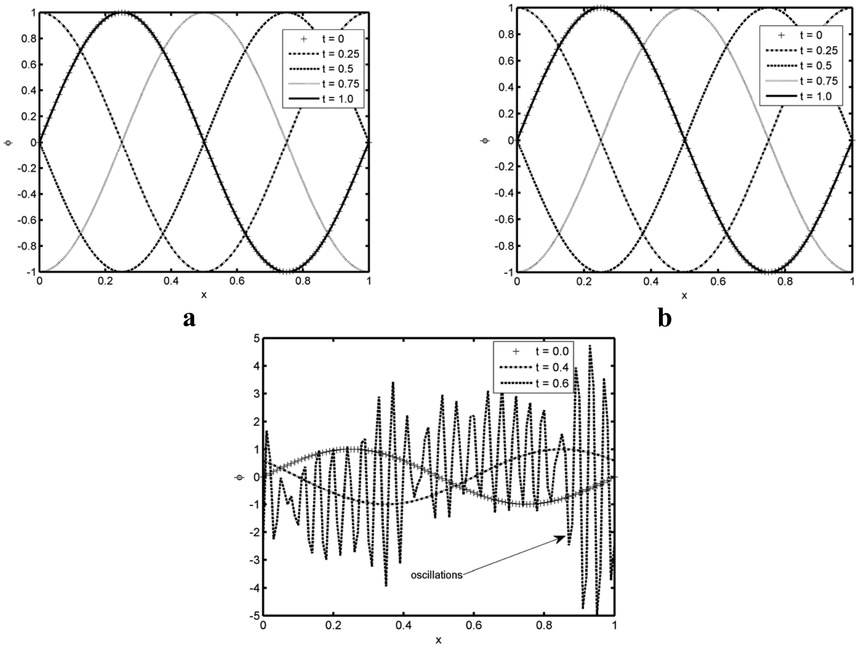

c

Figure 10: Solution of the 1^{st}-order wave equation by locally applied DQ method with the 1^{st} discretization scheme. a) for $r = 1$, the wave is preserved, b) for $r = 0.5$, the wave is preserved, c) for $r = 2$, oscillations are observed.

This scheme is consistent as $\phi_{,t} - a\phi_{,x} \rightarrow 0$, as h and $t \rightarrow 0$. It is noted from Eq. (52) that for the positive wave speed, a, there is some negative dissipation effect (dissipation removal from the system) which may not be completely avoided. In other words, even if this scheme is stable from the stability aspects, there is going to be some negative dissipation effect from the consistency point of view if the wave speed a is positive, and positive dissipation effect if the wave speed is negative. This observation is verified by numerically solving the 1^{st}-order wave equation using this scheme. For $r = 0.2$, the results are stable as the stability condition, as given by Eq. (43), is satisfied but the slight instability is added due to the negative dissipation effect as shown in Fig. 11a. For $r = 0.5$, as shown in Fig. 11b, the result gets unstable as the stability condition is violated.

For the forward time and central space scheme (scheme 5) given in Eq. (44), the discretization equation using Taylor series expansion [Mulay, Li and See (2009)] is

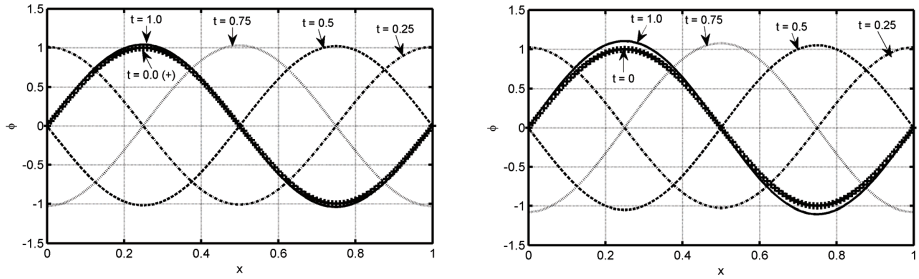

Figure 11: Solution of 1^{st}-order wave equation with the domains discretized by 4^{th}-scheme a) for $r = 0.2$, slight dispersion is observed, b) for $r = 0.5$, the oscillations are observed.

written as (Please refer Appendix C),

$$\phi_{,t} - a\phi_{,x} = \phi_{,xx}\left[\frac{h^2}{t} - \frac{ahr}{2}\right] \tag{53}$$

This scheme is consistent as $\phi_{,t} - a\phi_{,x} \to 0$, as h and $t \to 0$. As $\phi_{,xx}$ indicates the dissipation with respect to the space domain, it's desirable to have a positive or zero value for its coefficient. As such,

$$\left[\frac{h^2}{t} - \frac{ahr}{2}\right] \geq 0 \tag{54}$$

simplifying Eq. (54) results in,

$$|r| \leq \sqrt{2} \tag{55}$$

Eq. (55) gives the constraint on r from the consistency point of view. Comparing Eq. (48) with Eq. (55) it is clear that if the stability condition $|r| \leq 1$ is satisfied, automatically the consistency condition $|r| \leq \sqrt{2}$ is also satisfied but the vice a versa is not true hence, the stability condition is taken as the main stability criterion. This scheme is numerically implemented to solve the 1^{st}-order wave equation. For $r = 1$, the results are stable as shown in Fig.12a and the initial wave is preserved for all the time steps. For $r = 0.5$, the dissipation effect is observed as shown in Fig. 12b, which is expected from the consistency results though the results are stable. For $r = 2$, the instability is observed as shown in Fig. 12c due to the violation of both the stability and consistency conditions.

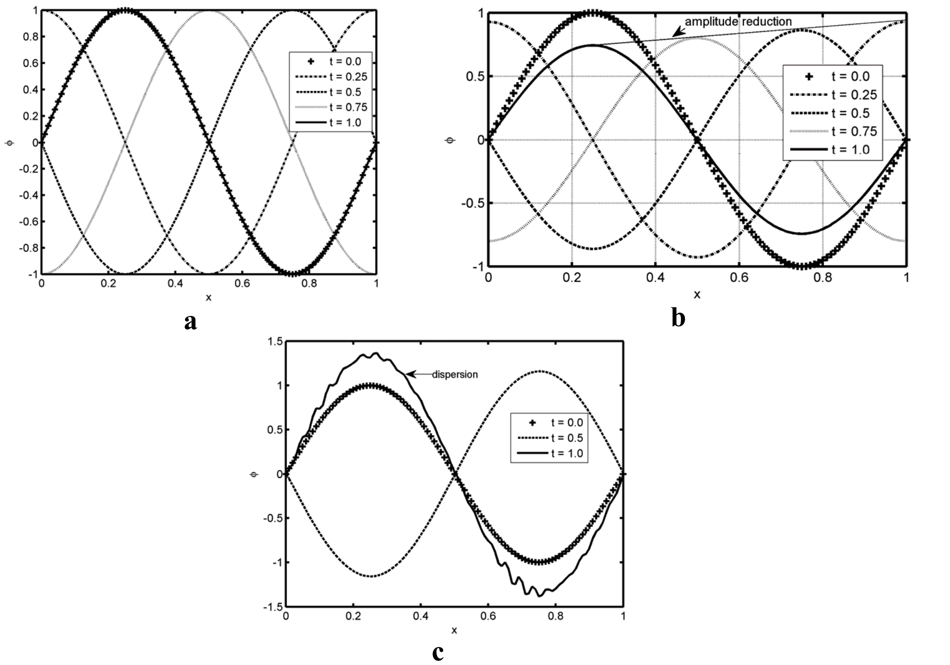

Figure 12: Solution of the 1^{st}-order wave equation by locally applied DQ method with the 5^{th} discretization scheme. a) for $r = 1$, the wave is preserved, b) for $r = 0.5$, numerical damping is observed, c) for $r = 2$, oscillations are observed.

All the stable schemes studied in the previous section are analyzed for the consistency in this section. The consistency and stability analyses analytical results are successfully verified by numerically solving the 1^{st}-order wave equation by the locally applied DQ method. It is observed that the numerical behaviour of the method is similar to what was predicted analytically. In the next section, the 1^{st}-order wave equation is solved by the RDQ method using Scheme 5.

3.3 The RDQ method implementation to solve the 1^{st}-order wave equation by the forward time and central space scheme (scheme 5)

In this section, the RDQ method is implemented to solve the wave equation by the forward time and central space scheme (scheme 5 given in Section 3.1.5).

A local interpolation domain is created around each virtual node as shown in Fig. 1, in which the field nodes falling are taken into consideration for the central virtual node function value approximation. A local domain is created around each field node, in which the field nodes falling are taken into consideration for the central field node function value approximation. At first, the unknown field node nodal parameters are computed at the time $t = 0$ by the initial condition,

$$\{\phi\}^0_{M\times 1} = [N]_{M\times M}\{U\}^0_{M\times 1} \tag{56}$$

where M is the total field nodes in whole domain, 0 indicates $t = 0$, $\{\phi\}^0_{M\times 1}$ is a known field node function values vector at the time $t = 0$, $[N]_{M\times M}$ is a shape function matrix representing the field node function values interpolation by the surrounding field nodes, $\{U\}^0_{M\times 1}$ is the unknown field node nodal parameters vector at $t = 0$. The virtual nodes function values at $t = 0$ are given as,

$$\{\phi\}^0_{N\times 1} = [N]_{N\times M}\{U\}^0_{M\times 1} \tag{57}$$

where N is the total virtual nodes in a whole domain, $\{\phi\}^0_{N\times 1}$ is the unknown virtual node function values vector at $t = 0$, $[N]_{N\times M}$ is a shape function matrix interpolating the virtual node function values in the form of surrounding field nodes, $\{U\}^0_{M\times 1}$ is the field node nodal parameters vector, which is computed by Eq. (56). After Eqns. (56) and (57) are computed, the virtual node function values vector for all the time increments is computed by,

$$\{\phi\}^t_{N\times 1} = [A]_{N\times N}\{\phi\}^{t-1}_{N\times 1} \tag{58}$$

where $[A]_{N\times N}$ is a discretization scheme coefficient matrix from Eq. (47), $\{\phi\}^t_{N\times 1}$ and $\{\phi\}^{t-1}_{N\times 1}$ are the virtual nodes function value vectors at the time t and $t-1$, respectively. After computing all virtual node function values, Eqns. (57) and (56) are used successively to compute the unknown field node nodal parameters and function values, respectively.

3.4 Comments on the 1st-order wave equation solution by the RDQ method

As explained in the earlier section, the 1st-order wave equation is solved by the RDQ method with the virtual and field nodes distributed in the cosine and uniform manner, respectively. The numerical results are analyzed by the wave equation consistency condition. The wave equation in its discretized form is given as,

$$\left\{a_{j,j} \quad a_{j,j+1}\right\}\left\{\begin{matrix}\phi(x_i,t_j)\\ \phi(x_i,t_{j+1})\end{matrix}\right\} = a\left\{a_{i,i-1} \quad a_{i,i} \quad a_{i,i+1}\right\}\left\{\begin{matrix}\phi(x_{i-1},t_j)\\ \phi(x_i,t_j)\\ \phi(x_{i+1},t_j)\end{matrix}\right\} \tag{59}$$

If the time and space domains have virtual nodes distributed in the uniform and cosine manner, respectively, then Eq. (59) is modified by computing the DQ weighting coefficients accordingly,

$$\frac{1}{t}\left\{-1 \quad 1\right\}\left\{\begin{matrix}\phi(x_i,t_j)\\ \phi(x_i,t_{j+1})\end{matrix}\right\} = a\left\{a_{i,i-1} \quad a_{i,i} \quad a_{i,i+1}\right\}\left\{\begin{matrix}\phi(x_{i-1},t_j)\\ \phi(x_i,t_j)\\ \phi(x_{i+1},t_j)\end{matrix}\right\} \tag{60}$$

where t is the time increment. The final consistency equation, $Pu - P(h_x,h_y)u$, for the scheme 5 is given as,

$$\phi_{,t} - a\phi_{,x} - \phi_{,t} + a\phi_{,x}\left[\frac{Bh_2 - Ah_1}{at}\right] = \phi\left[\frac{1-A-B}{t}\right] + \phi_{,xx}\left[\frac{Ah_1^2 + Bh_2^2}{2t} + \frac{a^2t}{2}\right] \tag{61}$$

where h_1 and h_2 are the nodal spacings between the virtual nodes ϕ_m^n and ϕ_{m-1}^n, and ϕ_m^n and ϕ_{m+1}^n, respectively, and A and B are the constants given as $A = \frac{1}{2} + \frac{ata_{i,i}}{2} + ata_{i,i-1}$ and $B = \frac{1}{2} + \frac{ata_{i,i}}{2} + ata_{i,i+1}$, respectively. Following conditions are derived for Eq. (61) to be consistent,

$$\frac{Bh_2 - Ah_1}{at} = 1, \quad \frac{1-A-B}{t} = 0 \text{ and } \left[\frac{Ah_1^2 + Bh_2^2}{2t} + \frac{a^2t}{2}\right] \geq 0 \tag{62}$$

to give a positive or zero dissipation.

Eq. (62) is the consistency constraints, which when satisfied gives the consistent wave equation discretization by the uniform and cosine distributions of virtual nodes in the time and space domains, respectively.

When the wave equation is solved by the RDQ method with the domain discretized by uniform and random field nodes, and uniform virtual nodes, respectively, Eq. (62) is exactly satisfied, which shows that the wave equation is consistently discretized as shown in Fig. 13. Also, it is observed that the numerical function values approach the corresponding analytical values as the field node spacing approaches the virtual node spacing. This result is important as it ensures that the RDQ method is convergent.

When the wave equation is solved by the RDQ method with the uniform and random field nodes in the computational domain, and uniform and cosine distributions of the virtual nodes in the time and space domains, respectively, Eq. (62) is not fully satisfied. This clearly shows that some dissipation is involved when the virtual nodes are cosine distributed in the space domain. This can be verified by plotting the numerical and analytical values at node $x = 1$ as shown in Fig. 14.

In this section, for the stable wave equation discretization, several single and multi-step schemes are studied and the stable schemes are identified. Further, the stable schemes are studied for their consistency while discretizing the wave equation. The

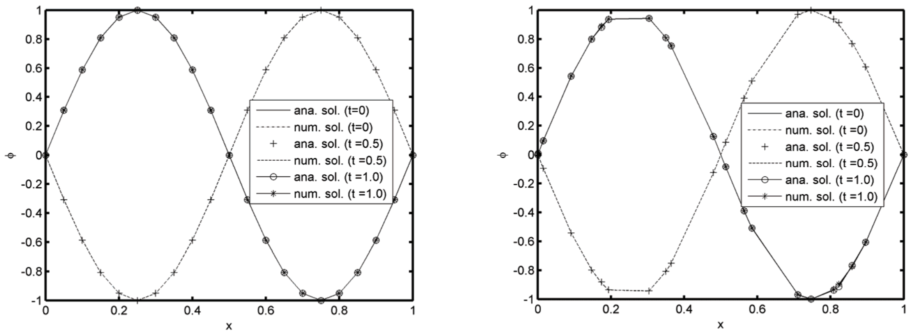

a **b**

Figure 13: The numerical and analytical function values comparison for the 1^{st}-order wave equation solved by the RDQ method with uniform virtual and a) uniform field nodes, b) random field nodes, respectively.

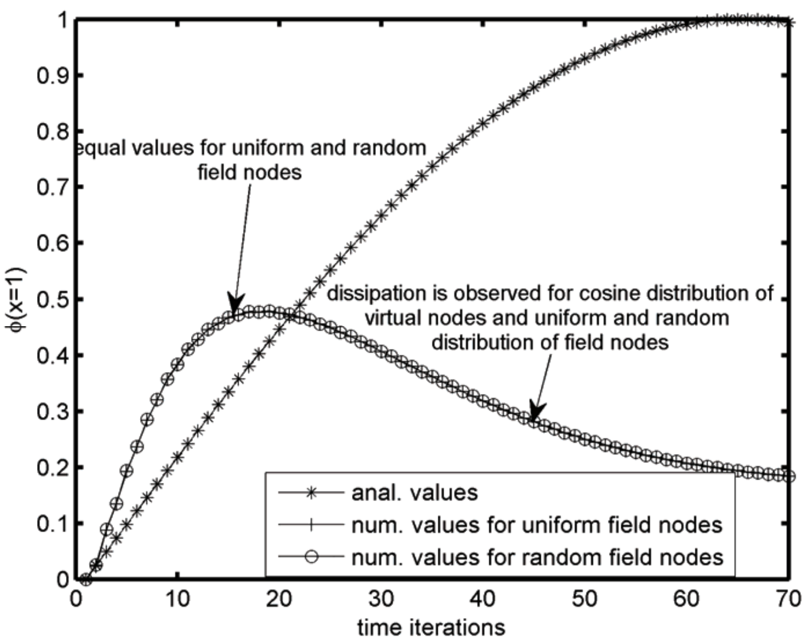

Figure 14: The time history plot of numerical and analytical function values comparison at the field node $(1,t)$ using the cosine virtual nodes distribution and uniform and random field node distributions, respectively, in the space domain.

stable schemes' analytically predicted behaviours are numerically verified by solving the wave equation using the locally applied DQ and RDQ methods. For the 5^{th} scheme it is seen that the numerical dissipation is involved when the wave equation is solved by the RDQ method with the cosine distribution of virtual nodes in the space but the wave is preserved during all the time steps for the uniform distribution of virtual nodes in the space domain. It is also observed that for the RDQ method coupled with the stable scheme and the domain discretized by uniform or random field nodes combined with the uniform virtual nodes, the initial wave is preserved during all the time steps. This is a very important result which highlights the applicability of the RDQ method with the domain discretized by random field nodes.

4 Transient heat conduction equation stability analysis

In this section, the transient heat conduction equation, $\frac{\partial u}{\partial t} = \alpha \frac{\partial^2 u}{\partial x^2}$, where α is the materials thermal conductivity, is analyzed for its stability and consistency, and numerically solved by the RDQ method with the domain discretized by either the uniform or random field nodes.

4.1 Forward time and space scheme

In this scheme, three and two virtual nodes are used in the space and time stencils, respectively, as shown in Fig. 7. The transient heat conduction equation is discretized at the uniformly distributed virtual nodes in the time and space domains with the weighting coefficients computed by Shu's general approach and given as,

$$\frac{\partial u(x_i,t_j)}{\partial t} = \alpha \frac{\partial^2 u(x_i,t_j)}{\partial x^2} \Rightarrow [u(x_i,t_{j+1}) - u(x_i,t_j)] = \frac{\alpha k}{h^2}\left[u(x_i,t_j) - 2u(x_{i+1},t_j) + u(x_{i+2},t_j)\right] \tag{63}$$

where k and h are the virtual node spacings in the temporal and spatial domains, respectively. The terms u in Eq. (63) are substituted by Taylor series [Mulay, Li and See (2009)], and simplified to give the transient heat conduction equation in the discretized form as (please refer Appendix C),

$$u_{,t} - \alpha u_{,xx} = \frac{-k}{2} u_{,tt} - 2\alpha h u_{,xxx} \tag{64}$$

The terms, $u_{,tt}$ and $u_{,xxx}$, represent the dissipation with respect to the time and space domains, respectively, and it can be seen from Eq. (64) that both the dissipation terms have negative coefficients, which means that there is going to be negative dissipation (dissipation removal from the system) and thus this scheme is not stable.

As the heat conduction equation is inconsistently discretized, there is no need to carry out the stability analysis. Hence, it is concluded that this scheme is unstable.

The heat conduction equation has the diffusion behaviour so that the field node temperature values are governed by the boundary conditions. This can be captured by considering both, the left and right, sides' domain nodes in the space discretization stencil. In the next section therefore, the space stencil is changed and the spatial discretization is carried out by considering the virtual nodes on both sides of the central virtual node.

4.2 Forward time and central space scheme

In this section, the forward time and central space scheme is used to discretize the transient heat conduction equation using the uniform and cosine distributions of virtual nodes in the space with the domain discretized by uniform and random field nodes. At first, the stability analysis is carried out for the uniform distribution of virtual nodes in the space then its consistency analysis is performed and the temporal spacing k operational range is obtained by combining both the results. The consistency analysis is then performed for the virtual nodes cosine distribution in the space and the constraint on k is derived, which gives the stable discretization. Next, the transient heat conduction equation is numerically solved using the RDQ method consisting of the uniform or cosine virtual node distributions combined with the uniform or random field node distributions in the space, their results are compared with the exact and FEM solutions.

4.2.1 The forward time and central space scheme stability analysis

In this scheme, three and two virtual nodes are considered for the space and time domains discretization stencils, respectively, as shown in Fig. 9a. The discretized heat conduction equation using the RDQ method is given as,

$$[u(x_i,t_{j+1})-u(x_i,t_j)] = \frac{\alpha k}{h^2}[u(x_{i-1},t_j)-2u(x_i,t_j)+u(x_{i+1},t_j)] \tag{65}$$

The inverse Fourier transform is performed on Eq. (65) and its characteristic or amplification polynomial is given as (Please refer Appendix A),

$$\phi(\theta) = 1-4m\sin^2\left(\frac{\theta}{2}\right) \tag{66}$$

where $m=(\alpha k)/h^2$. It is observed in Eq. (66) that $|\phi| \leq 1$ for $m \leq 1/2$ thus,

$$m = \frac{1}{2} \leq \frac{\alpha k}{h^2} \Rightarrow k \leq \frac{h^2}{2\alpha} \tag{67}$$

Eq. (67) is the stability condition for this scheme. For $0 \leq m \leq 1/2$, the graph of $|\phi|^2$ versus θ/π is plotted, as shown in Fig. 15a, and it is seen that all the roots, $\phi(\theta)$, from Eq. (66) are less that or equal to one. Hence, this scheme is stable with Eq. (67) as the stability condition.

4.2.2 The forward time and central space scheme consistency analysis

The discretized transient heat conduction equation is given by Eq. (65), the function terms u in Eq. (65) are substituted by Taylor series [Mulay, Li and See (2009)], simplifying it results in (please refer Appendix C),

$$u_{,t} - \alpha u_{,xx} = \frac{\alpha h^2}{12} u_{,xxxx} - \frac{k}{2} u_{,tt} - \frac{k^2}{2} u_{,ttt} \tag{68}$$

where h and k are the space and time domains virtual node spacings, respectively. In Eq. (68), $u_{,xxxx}, u_{,tt}$ and $u_{,ttt}$ represent dispersion in the space, and dissipation and dispersion in the time domains, respectively. The dissipation in the time domain term can be replaced as $u_{,tt} = \alpha^2 u_{,xxxx}$ thus,

$$u_{,t} - \alpha u_{,xx} = \frac{\alpha h^2}{12} u_{,xxxx} - \frac{k\alpha^2}{2} u_{,xxxx} - \frac{k^2}{2} u_{,ttt} \tag{69}$$

In order to make the dispersion $u_{,xxxx}$ less than or equal to zero,

$$\left[\frac{\alpha h^2}{12} - \frac{k\alpha^2}{2}\right] \leq 0 \Rightarrow \quad k \geq \frac{h^2}{6\alpha} \tag{70}$$

Eq. (70) is the stability condition on k from the consistency analysis. If we compare Eqns. (67) and (70), it is seen that $\left(h^2/6\alpha\right) \leq k \leq \left(h^2/2\alpha\right)$ is the temporal spacing operational range to give the stable solution.

4.2.3 The forward time and central space scheme consistency analysis using the cosine virtual nodes distribution in the space domain

The RDQ method uses the cosine distribution of virtual nodes to discretize the governing equation hence, it is crucial to understand its stability behaviour using the cosine distributed virtual nodes. For the cosine virtual nodes, spatial spacing h is not constant but changes at each node as,

$$x_i = x_0 + \frac{1}{2}\left[1 - \cos\left(\frac{i-1}{NP-1}\pi\right)\right] L \text{ for } i = 1, 2, \ldots, NP \tag{71}$$

where, x_0 and x_i are the starting and i^{th} virtual node domain co-ordinates, L and NP are the domain length and total virtual nodes, respectively. The discretized heat conduction equation using the cosine virtual nodes is given as,

$$u_{,t} - \alpha u_{,xx} = \frac{\alpha}{3}(h_2 - h_1)u_{,xxx} + \alpha \left[\frac{h_1^2 - h_1 h_2 + h_2^2}{12} - \frac{k\alpha}{2}\right] u_{,xxxx} \tag{72}$$

where $h_1 = x_i - x_{i-1}$ and $h_2 = x_{i+1} - x_i$. In order to keep the dispersion term $u_{,xxxx} \leq 0$,

$$k \geq \left[\frac{h_1^2 - h_1 h_2 + h_2^2}{6\alpha}\right] \tag{73}$$

The temporal spacing k is computed at each virtual node by Eq. (73) and the lowest value is chosen among them to get the stable solution. Hence, Eq. (73) is a stability condition for the cosine virtual nodes.

4.2.4 The RDQ method numerical implementation to solve the transient heat conduction equation

In this section, the RDQ method is implemented to solve the transient heat conduction equation with the cosine and uniformly distributed virtual nodes in the space, combined respectively with the domain discretized by the uniform and random field nodes, respectively. Their results are compared with the exact and FEM solutions, respectively. It is shown that the RDQ method results are closely matching with the exact and FEM solutions.

The governing equation is discretized at the internal domain virtual nodes with the space discretized by uniform virtual nodes combined with the uniform and random field nodes in the domain,

$$u_i^{n+1} = m\left(u_{i-1}^n + u_{i+1}^n\right) + (1-2m)u_i^n, \text{ where } i = 1,2,...,NP \tag{74}$$

$$\frac{\partial u}{\partial t}(1,t) = 0 \Rightarrow u_{NP}^n = \frac{2}{3}\left(2u_{NP-1}^n - \frac{u_{NP-2}^n}{2}\right) \tag{75}$$

where NP are the total virtual nodes in the domain and n indicates the n^{th} time step. Eq. (75) is used to impose the Neumann boundary condition at the virtual node $(x = 1)$. Note that both sides of Eq. (75) are at n^{th} time level.

The governing differential equation, the initial and boundary conditions are given as,

$$\frac{\partial u}{\partial t} = \frac{\partial^2 u}{\partial x^2} \text{ for } 0 \leq x \leq 1 \tag{76}$$

$$u(x,0) = 1.0, \quad u(0,t) = 0.0 \text{ and } \frac{\partial u}{\partial t}(1,t) = 0.0 \tag{77}$$

At the beginning, $t = 0$, the field and virtual nodes initial temperature values are computed using Eq. (77), and the left and right side domain boundary condition values are computed by Eqns. (77) and (75), respectively. Let $total\_it = T/k$ be the total time iterations and T be the total simulation time, then from $n = 1$ to $total\_it$, Eq. (74) is applied to compute the temperature values at all virtual nodes, the unknown field node parameter values are computed by $[S]_{NP\times N}\{U\}_{N\times 1}^{n+1} = \{u\}_{NP\times 1}^{\mathrm{n}+1} \Rightarrow \{U\}_{N\times 1}^{n+1}$, where $[S]_{NP\times N}$ is a shape function matrix approximating the virtual nodes, $\{u\}_{NP\times 1}^{\mathrm{n}+1}$, by the surrounding field nodes, $\{U\}_{N\times 1}^{n+1}$ is the field node parameters vector at $(n+1)^{th}$ time level, and NP and N are the total virtual and field nodes, respectively. Next, the field node temperature values are computed by $\left\{u_f\right\}_{N\times 1}^{n+1} = [S]_{N\times N}\{U\}_{N\times 1}^{n+1}$, where $[S]_{N\times N}$ is the shape function matrix interpolating the field nodes by surrounding field nodes, $\left\{u_f\right\}_{N\times 1}^{n+1}$ is the field node temperature values vector at $(n+1)^{th}$ time level. For the uniform and cosine virtual nodes, Eq. (70) and Eq. (73), respectively, are used to compute the temporal spacing, k.

As the FEM solution provided by Reddy (1993) is computed by four quadratic elements, for a comparison purpose, the RDQ method results are also computed by 9 field nodes (uniform and random). The transient temperature distribution at field node, $(x = 1)$, is computed by uniform and cosine virtual node distributions in the space with the space domain discretized by uniform and random field nodes, respectively, and compared with the exact and FEM solutions as shown in Fig. 15b.

It is observed from Fig. 15b that the RDQ method solutions are closely matching with the exact and FEM solutions, respectively, and accurate results are obtained with the randomly scattered field nodes in the domain. When this problem is solved by 31 uniform and 21 random field nodes scattered in the domain and combined with the cosine and uniform virtual nodes respectively, the diffusion for the time $t = 0$ to 1 sec. is shown in Figs. 16 and 17.

It is seen from Figs. 16b and 17b that the diffusion is well captured by the randomly scattered field nodes in the domain.

In this section, for the transient heat conduction equation, two different time and space discretization schemes are studied for the stability, out of them the forward time and central space scheme is found to be stable. The stable scheme is analyzed for its consistency with the domain discretized by uniform and cosine virtual nodes separately and the stability conditions are derived in Eqns. (70) and (73), respectively. This problem is solved using the locally applied DQ and RDQ methods with the uniform and random field nodes scattered in the domain, and it is demonstrated that the RDQ results are closely matching with the exact and FEM solutions, respectively, as seen in Fig. 15b.

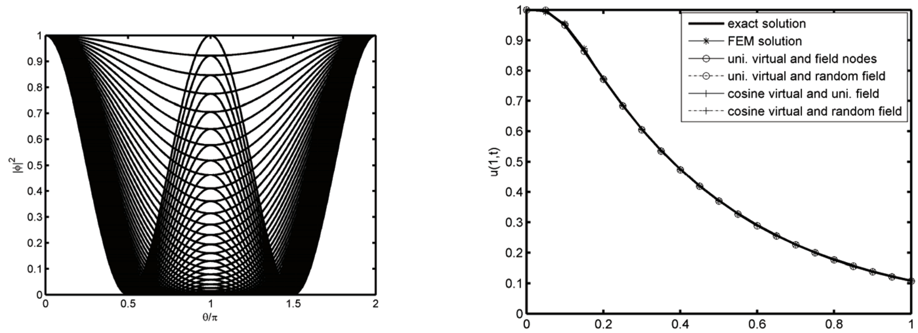

a **b**

Figure 15: a) The $|\phi|^2$ versus θ/π plot for the transient heat conduction problem using $0 \leq m \leq 0.5$ with the forward time and central space stencil as shown in Fig. 9a, b) Temperature time history plot at field node $(1,t)$ and its comparison with the exact and FEM solutions. The transient heat conduction problem is solved using the RDQ method with the uniform and cosine virtual nodes in the space respectively coupled with the uniform and randomly scattered field nodes.

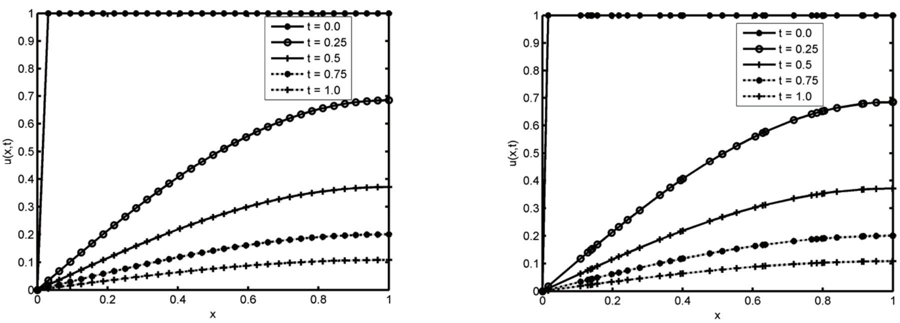

a **b**

Figure 16: The heat diffusion from $t = 0$ to 1 sec. by a) uniform field and virtual nodes, respectively, b) random field and uniform virtual nodes.

5 Transverse beam deflection equation stability analysis

In this section, the fixed-fixed beam transverse motion is studied using Euler-Bernoulli beam equation, $\rho A \frac{\partial^2 v}{\partial t^2} + EI \frac{\partial^4 v}{\partial x^4} = 0$, where ρ, A, E and I are the material density, cross sectional area, modulus of elasticity and the moment of inertial of the beam, respectively. This is accomplished by performing its stability and consistency analyses. The problem is then numerically solved by the RDQ method, by

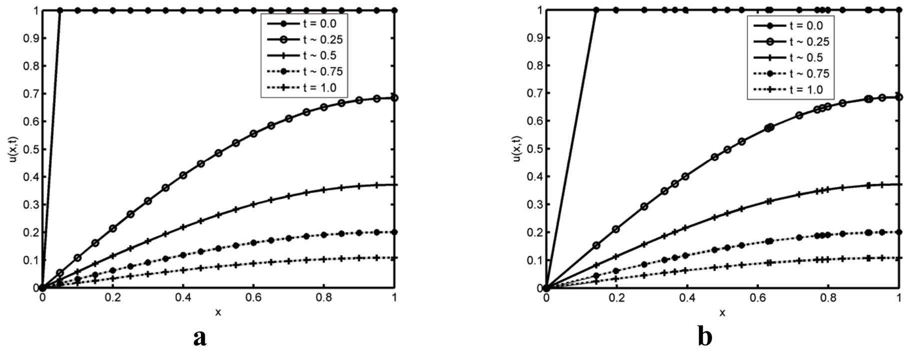

Figure 17: The heat diffusion from $t = 0$ to 1 sec. by a) uniform field and cosine virtual nodes, b) random field and cosine virtual nodes.

the temporal spacing k obtained from the stability and consistency analyses, for the free vibrations case and it is shown that the numerical results are closely matching with the analytically predicted values. The space and time discretizations are performed by both the explicit and implicit approaches and it is shown that an explicit approach adds the numerical dispersion thus, the successive deflection values ratio is more than 1 which leads to the instability. Where as, an implicit approach adds numerical dissipation thus, the successive deflection values ratio is less than 1, which is the stable solution.

5.1 An explicit approach to solve the transverse beam deflection equation

In this approach, the time and space derivatives from the governing differential equation are discretized by the forward time and central space approach as shown in Fig. 18. The discretized beam equation at the virtual node (x_i, t_j) by the RDQ method is given as,

$$(w_{i,j})^m = m\left[a_{i,j}(w_{i,i})^{m-1} - \frac{(w_{i,j})^{m-1}}{x_i - x_j}\right] \text{ and } (w_{i,i})^m = -\sum_{k=1,k\neq i}^{N_p}(w_{i,k})^m \tag{78}$$

where m is the derivative order, x_i and x_j are the nodal co-ordinates at i^{th} and j^{th} virtual node, respectively, N_p are the total DQ local domain virtual nodes for the virtual node (x_i, t_j), and $a_{i,j}$ are the 1^{st}-order derivative weighting coefficients.

$$\begin{Bmatrix} b_{j,j} & b_{j,j+1} & b_{j,j+2} \end{Bmatrix} \begin{Bmatrix} v_i^j \\ v_i^{j+1} \\ v_i^{j+2} \end{Bmatrix} +$$

$$\frac{EI}{\rho A}\left\{(w_{i,i-2})^4 \quad (w_{i,i-1})^4 \quad (w_{i,i})^4 \quad (w_{i,i+1})^4 \quad (w_{i,i+2})^4\right\}\begin{Bmatrix} v_{i-2}^j \\ v_{i-1}^j \\ v_i^j \\ v_{i+1}^j \\ v_{i+2}^j \end{Bmatrix} = 0 \tag{79}$$

The 4^{th}-order DQ weighting coefficients in Eq. (79) are computed by recursively applying Eq. (78) with $m = 4$. The final discretization equation is given as,

$$\left\{1 \quad -2 \quad 1\right\}\begin{Bmatrix} v_i^j \\ v_i^{j+1} \\ v_i^{j+2} \end{Bmatrix} + \frac{EIk^2}{\rho A h^4}\left\{1 \quad -4 \quad 6 \quad -4 \quad 1\right\}\begin{Bmatrix} v_{i-2}^j \\ v_{i-1}^j \\ v_i^j \\ v_{i+1}^j \\ v_{i+2}^j \end{Bmatrix} = 0 \tag{80}$$

where, k and h are the temporal and spatial spacings, respectively. Eq. (80) is further used for the stability and consistency analyses as explained in the next sections. It is seen from Eq. (80) that it is same as the finite difference equation.

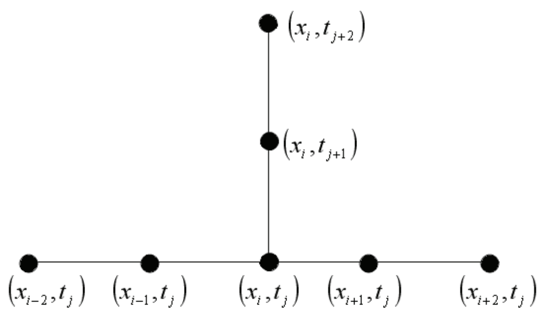

Figure 18: The time and space stencils for the transverse beam deflection problem by the explicit approach.

5.1.1 The explicit scheme stability analysis

In this section, the stability analysis of the explicit approach is carried out using Eq. (80), which can be rearranged as,

$$v_i^{j+2} = 2v_i^{j+1} - (1+6M)v_i^j + M(4v_{i-1}^j - v_{i-2}^j + 4v_{i+1}^j - v_{i+2}^j) \tag{81}$$

where $M = (EIk^2)/(\rho A h^4)$. After taking the inverse Fourier transform, the characteristic polynomial is given as (Please refer Appendix A),

$$\phi(z) = z^2 - 2z - [4M\cos(\theta)(2-\cos(\theta)) + 1 + 4M] \tag{82}$$

The roots, ϕ_+ and ϕ_-, of Eq. (82) are plotted by $0 \leq M \leq 1\times 10^{-5}$ as shown in Fig. 19, and it is seen that the maximum values are close to 1 for $M = 1\times 10^{-5}$ thus,

$$k \leq \sqrt{\frac{1\times 10^{-5}\rho A h^4}{\mathrm{EI}}} \tag{83}$$

Eq. (83) is the stability condition for the beam deflection using the explicit approach.

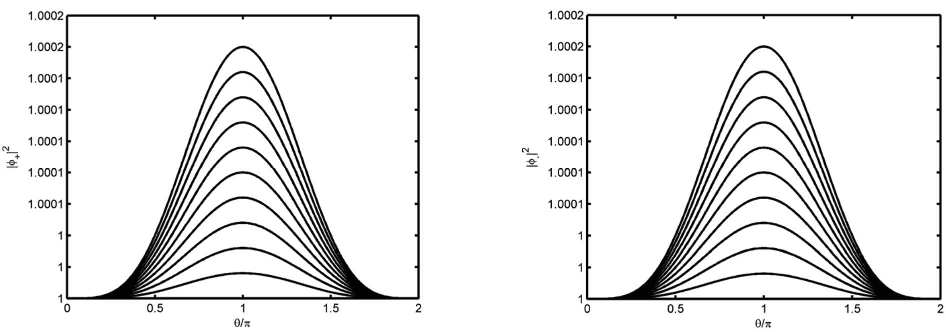

a **b**

Figure 19: For the transverse beam deflection by the explicit approach a) $|\phi_+|^2$ versus $\frac{\theta}{\pi}$ plot, b) $|\phi_-|^2$ versus $\frac{\theta}{\pi}$ plot.

5.1.2 The explicit approach consistency analysis

Beginning with Eq. (80), the terms v are replaced by corresponding Taylor series expansion [Mulay, Li and See (2009)] and the discretized equation is given as (please refer Appendix C),

$$mv_{,tt} + EIv_{,xxxx} = -mkv_{,ttt} - EIh^2 v_{,xxxxxx} \tag{84}$$

where $m = \rho A$. It is seen from Eq. (84) that the time and space discretizations are 1^{st}- and 2^{nd}-order accurate, respectively. The $v_{,ttt}$ and $v_{,xxxxxx}$ terms represent the dissipation and dispersion with respect to the time and space, respectively and they have negative coefficients, which indicate that there is dissipation removal from the system with respect to the time and the dispersion removal with respect to the space. The h^2 term will be small and can be neglected hence, the final discretized equation is given as,

$$mv_{,tt} + EIv_{,xxxx} = -mkv_{,ttt} \tag{85}$$

It is seen from Eq. (85) that the original governing equation is consistently discretized as $k \rightarrow 0, mv_{,tt} + EIv_{,xxxx} \rightarrow 0$ but there is going to be some numerical dispersion. It is essential to know the analytical dispersion value so that it can be compared with the RDQ method numerical results thus, the natural frequency (ω_n) and the successive amplitude reduction ratio expressions are derived in the next section.

5.1.3 The natural frequency and amplitude reduction ratio computation

In this section, the fixed-fixed beam natural frequency is derived using the separation of variables method and subsequently, the amplitude reduction ratio is computed with the reference of Dominic and Damodaran (2009).

The $v(x,t)$ can be substituted as $v(x,t) = \psi(t)\xi(x)$, with this substitution, Eq. (85) is converted to the two ordinary differential equations (ODE) as,

$$\frac{1}{\psi}\left[k\frac{\partial^3\psi}{\partial t^3} + \frac{\partial^2\psi}{\partial t^2}\right] = -\omega_n^2 \tag{86}$$

$$\frac{\partial^4\phi}{\partial x^4} - \frac{m\phi}{EI}\omega_n^2 = 0 \tag{87}$$

where ω_n is the natural frequency of the system. Eqns. (86) and (87) give the deflection amplitude variations with respect to the time and space domains, respectively. Eq. (87) is solved to compute ω_n by assuming its general solution as a linear combination of trigonometric equations and $k_n^4 = (m\omega_n^2)/EI$,

$$\phi(x) = C_1\left[\cos(k_n x) + \cosh(k_n x)\right] + C_2\left[\cos(k_n x) - \cosh(k_n x)\right] +$$

$$C_3\left[\sin(k_n x) + \sinh(k_n x)\right] + C_4\left[\sin(k_n x) - \sinh(k_n x)\right] \tag{88}$$

using the fixed-fixed beam boundary conditions, $v(0) = 0.0$, $v(1.0) = 0.0, \partial v/\partial x(0) = 0.0$ and $\partial v/\partial x(1) = 0.0$, Eq. (88) is solved to obtain,

$$\cos(M)\cos(hM) = 1.0 \tag{89}$$

where $M = k_n L$. Eq. (89) is solved to get the M values as 4.73004074486 and 7.85320462. The first mode is selected thus,

$$M = k_n L = 4.73004074486 \Rightarrow \omega_n = 22.3733 \text{ rad / sec. for } L = 1 \tag{90}$$

Eq. (90) gives the natural frequency of the fixed-fixed beam. The ω_n value from Eq. (90) can be easily verified by considering few uniformly distributed virtual nodes and computing the spatial discretization matrix Eigen values using Eq. (80). Eq. (86) is used to compute the successive deflection amplitude reduction ratio with respect to the time. Eq. (86) roots are computed and the general solution is given as,

$$\psi(t) = e^{-\upsilon_1 t}\left[c_2 \sin(\omega_d t)\right] \tag{91}$$

where, $\omega_d = \left[\sqrt{3}/(24k)\right]\left[2\beta - (8/\beta)\right]$ is the damped natural frequency, and $\upsilon_1 = (1/12k)\left(\beta + 4/\beta - 4\right)$, where, $\beta = \sqrt[3]{-108\omega_n^2 k^2 - 8 + 12\sqrt{3}\left(\sqrt{27\omega_n^2 k^2 + 4}\right)\omega_n k}$. For $t = t_1$ to $(t_1 + 2\pi/\omega_d)$ i.e. for two successive peaks, the ratio, $\psi(t_1 + 2\pi/\omega_d)/\psi(t_1)$, by Eq. (91) is taken and simplified by the periodicity property of the sin function and given as,

$$ratio = \exp\left(\frac{-2\pi\upsilon_1}{\omega_d}\right) \tag{92}$$

Eq. (92) is used to compute the successive deflection amplitude reduction ratios using the explicit approach.

The transverse beam deflection problem is solved using an explicit approach with its governing equation, boundary and initial conditions as [Reddy (1993)],

$$\frac{\partial^2 v}{\partial t^2} + \frac{\partial^4 v}{\partial x^4} = 0 \text{ for } (0 \le x \le 1) \tag{93}$$

$$v(0,t) = 0.0, \quad v(1,t) = 0.0, \quad \frac{\partial v}{\partial x}(0,t) = 0.0 \text{ and } \frac{\partial v}{\partial x}(1,t) = 0.0 \tag{94}$$

$$v(x,0) = \sin(\pi x) - \pi x(1-x), \quad \frac{\partial v}{\partial x}(x,0) = 0 \tag{95}$$

It is seen from Eq. (94) that there are two boundary conditions at the left and right domain virtual nodes, respectively, thus, in order to have a single algebraic equation at each virtual node, one of the boundary conditions at the boundary virtual node are transferred to their neighbouring nodes as given [Li, Mulay and See (2009)],

$$\begin{aligned}
&\frac{\partial v}{\partial x}(0,t) = 0 = \frac{v_2 - v_1}{x_2 - x_1} \Rightarrow v_2(x_2,t) = 0.0, \\
&\frac{\partial v}{\partial x}(1,t) = 0 = \frac{v_{NP-1} - v_{NP}}{x_{NP-1} - x_{NP}} \Rightarrow v_{NP-1}(x_{NP-1},t) = 0.0
\end{aligned} \tag{96}$$

where, NP are the total virtual nodes and the suffices $1, 2, NP-1$ and NP indicate the virtual node numbers. The modified boundary conditions are given as,

$$v(0,t) = 0.0, \quad v(1,t) = 0.0, \quad v(x_2,t) = 0.0 \text{ and } v(x_{NP-1},t) = 0.0 \tag{97}$$

In Reddy (1993), this problem is solved by 2 Euler-Bernoulli beam elements so, for a comparison purpose, here it is solved with 5 $(h = 0.25)$ uniform field and virtual nodes, respectively, and the temporal spacing $k = 2 \times 10^{-4}$ sec. is computed using Eq. (83). Initially, the problem is solved by the locally applied DQ and RDQ methods with the domain discretized by uniform and random field nodes and the deflection at the central field node $(0.5,t)$ is shown in Fig. 20a. It is seen from Fig. 20a that the field node $(0.5,t)$ deflection values are identical, which indicate that the RDQ method can effectively handle the random field nodes distribution. Next, the problem is solved using the RDQ method by uniform virtual nodes in the space with the domain discretized by uniform and random field nodes and their results are compared with the exact and FEM solutions, respectively, as shown in Fig. 20b. It is observed from Fig. 20b that there is a slight dispersion over the time as predicted from Eq. (85). The successive peak values at $t_1 = 0.1624$ sec. and $t_2 = 0.3248$ sec. are obtained from Fig. 20b and their ratio is found to be $v_2/v_1 = (0.2253)/(0.2199) \approx 1.0245$, the analytical amplitude reduction ratio, computed by Eq. (92), is found to be $ratio = \exp(-2\pi(-0.050058)/22.3723) \approx 1.014$ thus, it can be observed that the numerical amplitude reduction ratio is closely matching with the corresponding analytical value. It is also observed that $v_2/v_1 > 1$, which clearly indicates the dispersion in the solution. When this problem is solved with the lower temporal increment $k = 6.25 \times 10^{-5}$ sec., the numerical and analytical amplitude reduction ratios are found to be $v_2/v_1 \approx 1.007$ and 1.005, respectively, which are also closely matching with each other hence, it is concluded that $(v_2/v_1) > 1$ and $(v_2/v_1) \to 1.0$ as $k \to 0$ for the explicit approach.

5.2 Implicit approach to solve the transverse beam deflection equation

As seen from Eq. (83) that the explicit approach has stringent temporal spacing requirement thus, the computational cost is very high for large number of field nodes. Also, Eq. (85) shows that there is a dissipation reduction effect with the

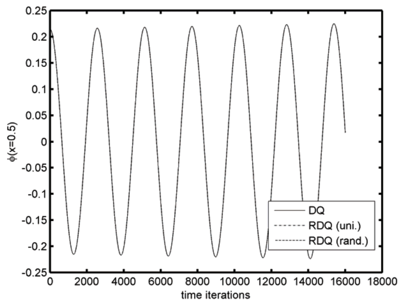

a

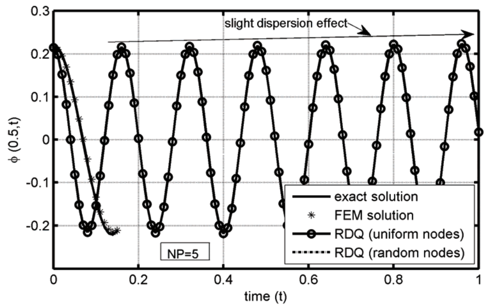

b

Figure 20: Time history plot of transverse deflection at the field node $(0.5, t)$ a) by the locally applied DQ, and RDQ methods combined with the uniform and random field nodes scattered in the domain, b) by the RDQ method separately combined with the uniform and random field node distributions and its comparison with the FEM and exact solutions.

time hence, the numerical beam deflection equation discretization is consistent only when $k \to 0$. In order to overcome these limitations, an implicit time discretization approach is studied in this section.

With the implicit approach, the space and time derivatives from the governing differential equation are discretized at the same time level as shown in Fig. 21a. The RDQ method discretization equation is given as,

$$\left\{ b_{j,j-2} \quad b_{j,j-1} \quad b_{j,j} \right\} \begin{Bmatrix} v_i^{j-2} \\ v_i^{j-1} \\ v_i^j \end{Bmatrix} +$$

$$\frac{EI}{\rho A} \left\{ (w_{i,i-2})^4 \quad (w_{i,i-1})^4 \quad (w_{i,i})^4 \quad (w_{i,i+1})^4 \quad (w_{i,i+2})^4 \right\} \begin{Bmatrix} v_{i-2}^j \\ v_{i-1}^j \\ v_i^j \\ v_{i+1}^j \\ v_{i+2}^j \end{Bmatrix} = 0 \tag{98}$$

The DQ weighting coefficients from Eq. (98) are computed using Shu's general approach and substituted to give,

$$\begin{Bmatrix} 1 & -2 & 1 \end{Bmatrix} \begin{Bmatrix} v_i^{j-2} \\ v_i^{j-1} \\ v_i^j \end{Bmatrix} + \frac{EIk^2}{\rho A h^4} \begin{Bmatrix} 1 & -4 & 6 & -4 & 1 \end{Bmatrix} \begin{Bmatrix} v_{i-2}^j \\ v_{i-1}^j \\ v_i^j \\ v_{i+1}^j \\ v_{i+2}^j \end{Bmatrix} = 0 \tag{99}$$

Rearranging Eq. (99) terms lead to,

$$v_i^j(1+6M) + M\left(v_{i-2}^j - 4v_{i-1}^j - 4v_{i+1}^j + v_{i+2}^j\right) = 2v_i^{j-1} - v_i^{j-2} \tag{100}$$

where $M = (EIk^2)/(\rho A h^4)$. When Eq. (100) is applied at all the internal domain virtual nodes, it results in the matrix which can be solved by any of the direct or iterative solvers.

5.2.1 The implicit approach consistency analysis

It is essential to know the numerically solved exact PDE by the implicit approach thus, after expanding the terms v by Taylor series [Mulay, Li and See (2009)] from Eq. (100), its consistency equation is given as (Please refer Appendix C),

$$mv_{,tt} + EIv_{,xxxx} = mkv_{,ttt} \tag{101}$$

where $m = \rho A$. It is seen from Eq. (101) that the numerical damping or dissipation is added with respect to the time but still the discretization is consistent because as $k \to 0, mv_{,tt} + EIv_{,xxxx} \to 0$ thus, with the temporal spacing reduction, the discretized governing PDE in Eq. (101) approaches its continuous form given in Eq. (93). In order to compute the analytical numerical dissipation, the successive amplitude reduction ratio equation, as also shown in [Dominic and Damodaran (2009)], is developed in the next section.

5.2.2 Amplitude reduction ratio computation for the implicit approach

As explained in Section 5.1.3, the terms, $v(x,t)$, from Eq. (101) are substituted by $v(x,t) = \psi(t)\xi(x)$ and it is converted to two ODEs,

$$k\frac{\partial^3 \psi}{\partial t^3} - \frac{\partial^2 \psi}{\partial t^2} - \omega_n^2 \psi = 0 \tag{102}$$

$$\frac{\partial^4 \phi}{\partial x^4} - \frac{m\phi}{EI}\omega_n^2 = 0 \tag{103}$$

where ω_n is the systems natural frequency. Eq. (102) is solved to compute the successive amplitude reduction ratios with the time. Eq. (102) roots are computed and the general solution is given as,

$$\psi(t) = e^{\upsilon_1 t}\left[c_2 \sin(\omega_d t)\right] \tag{104}$$

where $\omega_d = \left[\sqrt{3}/(24k)\right]\left[2\beta - (8/\beta)\right]$ is the damped natural frequency, and $\upsilon_1 = (1/12k)(-\beta - 4/\beta + 4)$, where $\beta = \sqrt[3]{108\omega_n^2k^2 + 8 + 12\sqrt{3}\left(\sqrt{27\omega_n^2k^2+4}\right)\omega_n k}$. For $t = t_1$ to $(t_1 + 2\pi/\omega_d)$ i.e. for two successive peaks, the ratio, $\psi(t_1 + 2\pi/\omega_d)/\psi(t_1)$, by Eq. (104) is taken and simplified by the sin function periodicity property as,

$$ratio = \exp\left(\frac{2\pi\upsilon_1}{\omega_d}\right) \tag{105}$$

Eq. (105) is used to compute the implicit approach successive amplitude reduction ratios.

The transverse beam deflection problem is solved using the implicit approach with its governing equation, initial and boundary conditions as given in Eqns. (93), (95) and (97), respectively. In order to compare the implicit approach results with the explicit approach one, the problem is solved by 5 uniform virtual nodes with the domain discretized by uniform and random field nodes, and $k = 2\times10^{-4}$ sec. Fig.21b shows the beam deflection problem comparison results by the RDQ method implicit approach with the FEM and exact solutions. It is seen from Fig. 21b that the field node $(0.5, t)$ deflection values are damping with the time as expected from Eq. (101), and identical results are obtained with the RDQ method using the uniform and random field nodes, which highlights that the RDQ method effectively handles the random field nodes distribution. The successive peak values are obtained from Fig. 21b and their ratio is found to be $v_2/v_1 = (0.2043)/(0.2094) \approx 0.9756$, the analytical amplitude reduction ratio computed by Eq. (105) is found to be $ratio = \exp(2\pi(\upsilon_1)/22.3723) \approx 0.9860$ thus, it can be observed that the numerical and analytical amplitude reduction ratios are closely matching. It is also observed that $v_2/v_1 < 1$, which clearly indicates the dissipation in the solution. When this problem is solved with the lower temporal increment $k = 6.25\times10^{-5}$ sec. similar to the explicit approach, the numerical and analytical amplitude reduction ratios are found to be $(v_2/v_1) \approx 0.992$ and 0.9956, respectively, which are also closely matching with each other hence, it is concluded that $(v_2/v_1) < 1$ and $(v_2/v_1) \to 1.0$ as $k \to 0$ for the implicit approach.

In summary, the transverse beam deflection stability analysis is carried out in this section using the explicit and implicit approaches. It is observed that to get the stable solution using the explicit approach, the temporal spacing has to be very small with increase in the field nodes, which results in high computational cost, and the numerical governing PDE discretization involves the negative dissipation as shown by Eq. (85). To overcome these problems, the implicit approach is used for the temporal discretization and it is found that the numerical governing PDE discretization is consistent with its continuous form with the numerical damping as shown by Eq. (101) and there is no direct constraint on the temporal spacing from the stability aspects. It is also shown for both the explicit and implicit approaches that the numerical successive amplitude reduction ratios are matching with their corresponding analytical values.

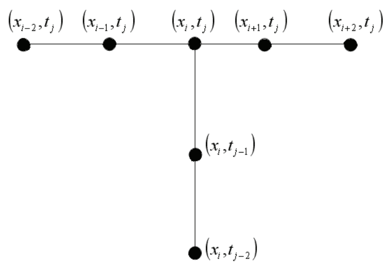

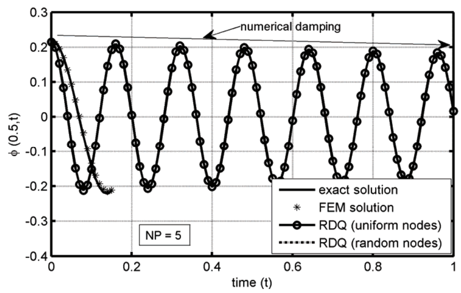

Figure 21: For the transverse beam deflection problem by the implicit approach a) time and space stencils, b) comparison of transverse deflection at the field node $(0.5,t)$ with the FEM and exact solutions by the RDQ method. The time and space domains are discretized by the implicit approach with the uniform virtual nodes respectively combined with the uniform and random field nodes.

6 Conclusions

The detailed stability analysis of a novel strong-form meshless method called the RDQ method is carried out in this paper. At the beginning, the RDQ method is presented with the fixed RKPM interpolation function combined with the locally applied DQ formulations. The 1^{st}-order wave equation stability analysis is performed for the five different single and multi-step schemes using the VN and Schur polynomials. The stable schemes are identified and are further analyzed for additional constraints on r based on the consistency analysis. The observations made from the stable schemes stability and consistency analyses are verified by numerically implementing them to solve the 1^{st}-order wave equation by the locally applied DQ (for Schemes 1, 4 and 5) and RDQ methods (for Scheme 5). The results are analyzed using the virtual nodes distributed in the uniform and cosine manners in the space domain. It is observed that some numerical dissipation is involved when the cosine virtual node distribution is used in the space domain. This observation is analytically verified by deriving the consistency constraint conditions for the scheme 5 as given in Eq. (62).

The transient heat conduction equation is solved by the forward time and central space stencil with the stable range of temporal spacing identified from the stability and consistency analyses. The heat conduction equation is solved with the uniform and cosine virtual node distributions in the space respectively coupled with the space discretized by uniform and random field node distributions, and their results at the field node $(0.5, t)$ are compared with the FEM and exact solutions, as shown in Fig. 15b. The temperature distributions from $t = 0$ to 1 sec. are plotted in Figs. 16 and 17, and it is seen that the results are almost identical; this indicates that the RDQ method is equally capable in handling the uniform and random field node distributions in the space.

The transverse beam deflection equation is solved by the RDQ method using the explicit and implicit approaches, and it is shown that even though the explicit approach consistently discretize the governing PDE, the numerical dispersion is involved which makes it numerically unstable. This is verified by comparing the numerical successive amplitude reduction ratios with the analytical values and observing that $(v_2/v_1) > 1$ and $(v_2/v_1) \rightarrow 1.0$ as k $\rightarrow 0$. The implicit approach consistently discretizes the governing PDE with a numerical damping but the solution is numerically stable. This is verified by comparing the numerical successive amplitude reduction ratios with the corresponding analytical values and observing that $(v_2/v_1) < 1$ and $(v_2/v_1) \rightarrow 1.0$ as $k \rightarrow 0$.

In summary, in the presented work, by several transient PDEs, a broad conceptual framework, based on the physical interpretation of mathematical terms, is developed with combining the stability and consistency analyses together to solve the transient PDEs. The approach can be successfully applied while solving any transient PDE.

Acknowledgement: The authors gratefully acknowledge the financial support from Sun Microsystems Inc. through a collaborative research with Nanyang Technological University, Singapore under the project number: M48050114.

References

Aceto, L.; Trigiante, D. (2007): The stability problem for linear multistep methods: Old and new results. *J Comput Appl Math*, vol. 210, pp. 2-12.

Aluru, N. R. (2000): A point collocation method based on reproducing kernel approximations. *Int J Numer Meth Eng*, vol. 47, pp. 1083-1121.

Aluru, N. R.; Li, G. (2001): Finite cloud method: a true meshless technique based on a fixed reproducing kernel approximation. *Int J Numer Meth Eng*, vol. 50, pp. 2373-2410.

Arefmanesh, A.; Najafi, M.; Abdi, H. (2008): Meshless Local Petrov-Galerkin Method with Unity Test Function for Non-Isothermal Fluid Flow. *CMES: Computer Modeling in Engineering and Sciences*, vol. 25, No. 1, pp. 9-22.

Ata, R; Soulaimani, A. (2005): A stabilized SPH method for inviscid shallow water flows. *Int J Numer Meth Fluid,* vol. 47, pp. 139-159.

Atluri, S. N. (2004): The meshless method (MLPG) for domain & BIE discretizations. Tech Science Press, Forsyth.

Atluri, S. N. (2005): Methods of computer modeling in engineering & the sciences. Tech Science Press, Forsyth.

Atluri, S. N.; Han, Z. D.; Rajendran, A. M. (2004): A new implementation of the meshless finite volume method, through the MLPG "mixed" approach. *CMES: Computer Modeling in Engineering and Sciences*, vol. 6, No. 6, pp. 491-513.

Atluri, S. N.; Liu, H. T.; Han, Z. D. (2006a): Meshless Local Petrov-Galerkin (MLPG) mixed collocation method for elasticity problems. *CMES: Computer Modeling in Engineering and Sciences*, vol. 14, No. 3, pp. 141-152.

Atluri, S. N.; Liu, H. T.; Han, Z. D. (2006b): Meshless Local Petrov-Galerkin (MLPG) mixed finite difference method for solid mechanics. *CMES: Computer Modeling in Engineering and Sciences*, vol. 15, No. 1, pp. 1-16.

Atluri, S. N.; Shen, S. (2002): The meshless local Petrov-Galerkin method. Tech Science Press, Encino.

Balsara, D. S. (1995) von Neumann Stability Analysis of Smoothed Particle Hydrodynamics-Suggestions for Optimal Algorithms. *J Comput Phys,* vol. 121, pp. 357-372.

Bellman, R.E.; Kashef, B.G.; Casti, J. (1972): Differential quadrature: a technique for the rapid solution of nonlinear partial differential equations. *J Comput Phys,* vol. 10, pp 40–52.

Belytschko, T.; Guo, Y.; Liu, W. K.; Xiao, S. P. (2000): A unified stability analysis of the meshless particle methods. *Int J Numer Meth Eng*, vol. 48, pp. 1359-1400.

Borve, S.; Omang, M; Trulsen, J. (2004): Two-dimensional MHD smoothed particle hydrodynamics stability analysis. *Astrophys J Suppl,* vol. 153, pp. 447-462.

Cai, Y. C.; Zhu, H. H. (2008): A Local Meshless Shepard and Least Square Interpolation Method Based on Local Weak Form. *CMES: Computer Modeling in*

Engineering and Sciences, vol. 34, No. 2, pp. 179-204.

Chen, S. S.; Liu, Y. H.; Cen, Z. Z. (2008): A Combined Approach of the MLPG Method and Nonlinear Programming for Lower-Bound Limit Analysis. *CMES: Computer Modeling in Engineering and Sciences*, vol. 28, No. 1, pp. 39-55.

Dang, T. D.; Sankar, B. V. (2008): Meshless Local Petrov-Galerkin Micromechanical Analysis of Periodic Composites Including Shear Loadings. *CMES: Computer Modeling in Engineering and Sciences*, vol. 26, No. 3, pp. 169-187.

Dominic, D. J. C.; Damodaran, M. (2009): Computational Fluid-Structure Interaction of a Flapping Wing in Free Flight Using Overlapping Grids. 27^{th} *AIAA Applied Aerodynamics Conference*, Texas, USA 22-25 June 2009; AIAA 2009-3849.

Fung, T.C. (2002): Stability and accuracy of differential quadrature method in solving dynamic problems. *Comput Meth Appl Mech Eng*, vol. 191, pp. 1311-1331.

Gingold, R. A.; Monaghan, J. J. (1977): Smoothed particle hydrodynamics: theory and application to non-spherical stars. *Mon Not Roy Astron Soc Lett*, vol. 181, pp. 375-389.

Han, Z. D.; Liu, H. T.; Rajendran, A. M.; Atluri, S. N. (2006): The applications of Meshless Local Petrov-Galerkin (MLPG) approaches in high-speed impact, penetration and perforation problems. *CMES: Computer Modeling in Engineering and Sciences*, vol. 14, No. 2, pp. 119-128.

Han, Z. D.; Rajendran, A. M.; Atluri, S. N. (2005): Meshless Local Petrov-Galerkin (MLPG) approaches for solving nonlinear problems with large deformations and rotations. *CMES: Computer Modeling in Engineering and Sciences*, vol. 10, No. 1, pp. 1-12.

Haq, S.; Siraj, U. I.; Ali, A. (2008): A Numerical Meshfree Technique for the Solution of the MEW Equation. *CMES: Computer Modeling in Engineering and Sciences*, vol. 38, No. 1, pp. 1-23.

Haq, S.; Siraj, U. I.; Uddin, M. (2009): Numerical Solution of Nonlinear Schrodinger Equations by Collocation Method Using Radial Basis Functions. *CMES: Computer Modeling in Engineering and Sciences*, vol. 44, No. 2, pp. 115-135.

Jarak, T.; Soric, J.; Hoster, J. (2007): Analysis of shell deformation responses by the meshless local Petrov-Galerkin (MLPG) approach. *CMES: Computer Modeling in Engineering and Sciences*, vol. 18, No. 3, pp. 235-246.

Jin, X.; Li, G.; Aluru, N. R. (2001): On the Equivalence Between Least-Squares and Kernel Approximations in Meshless Methods. *CMES: Computer Modeling in Engineering and Sciences*, vol. 2, No. 4, pp. 447-462.

Kosec, G.; Šarler, B. (2008): Local RBF Collocation Method for Darcy Flow. *CMES: Computer Modeling in Engineering and Sciences,* vol. 25, No. 3, pp. 197-207.

Le, P.; Mai-Duy, N.; Tran-Cong, T.; Baker, G. (2008): A Meshless Modeling of Dynamic Strain Localization in Quasi-Brittle Materials Using Radial Basis Function Networks. *CMES: Computer Modeling in Engineering and Sciences,* vol. 25, No. 1, pp. 43-66.

Li, S.; Atluri, S. N. (2008): Topology-optimization of Structures Based on the MLPG Mixed Collocation Method. *CMES: Computer Modeling in Engineering and Sciences,* vol. 26, No. 1, pp. 61-74.

Li, L.; Liu, S.; Wang, H. (2008): Meshless Analysis of Ductile Failure. *CMES: Computer Modeling in Engineering and Sciences,* vol. 36, No. 2, pp. 173-191.

Li, H.; Mulay, S. S.; See, S. (2009): On the Convergence of Random Differential Quadrature (RDQ) Method and Its Application in Solving Nonlinear Differential Equations in Mechanics. *CMES: Computer Modeling in Engineering and Sciences*, vol. 48, No. 1, pp. 43-82.

Liew, K. M.; Huang, Y. Q.; Reddy, J. N. (2003): Moving least squares differential quadrature method and its application to the analysis of shear deformable plates. *Int J Numer Meth Eng*, vol. 56, pp. 2331-2351.

Liew, K. M.; Huang, Y. Q.; Reddy, J. N. (2004): Analysis of general shaped thin plates by the moving least-squares differential quadrature method. *Finite Elem Anal Des*, vol. 40, pp. 1453-1474.

Liew, K. M.; Zhang, J. Z.; Ng, T. Y.; Meguid, S. A. (2003): Three-dimensional modelling of elastic bonding in composite laminates using layerwise differential quadrature. *Int J Solids Struct*, vol. 40, pp. 1745-1764.

Lisio, R. D.; Grenier, E.; Pulvirenti, M. (1998): The Convergence of the SPH Method. *Comput Math Appl,* vol. 35, pp. 95-102.

Liu, C. S. (2007a): A Meshless Regularized Integral Equation Method for Laplace Equation in Arbitrary Interior or Exterior Plane Domains. *CMES: Computer Modeling in Engineering and Sciences*, Vol. 19, No. 1, pp. 99-109.

Liu, C. S. (2007b): A MRIEM for Solving the Laplace Equation in the Doubly-Connected Domain. *CMES: Computer Modeling in Engineering and Sciences*, Vol. 19, No. 2, pp. 145-161.

Liu, Y. H.; Chen, S. S.; Li, J.; Cen, Z. Z. (2008): A Meshless Local Natural Neighbour Interpolation Method Applied to Structural Dynamic Analysis. *CMES: Computer Modeling in Engineering and Sciences*, Vol. 31, No. 3, pp. 145-156.

Liu, W. K.; Jun, S.; Zhang, Y. F. (1995): Reproducing Kernel Particle Methods.

Int J Numer Meth Fluid, vol. 20, pp. 1081-1106.

Long, S. Y.; Liu, K. Y.; Li, G. Y. (2008): An Analysis for the Elasto-Plastic Fracture Problem by the Meshless Local Petrov-Galerkin Method. *CMES: Computer Modeling in Engineering and Sciences*, vol. 28, No. 3, pp. 203-216.

Lucy, L. B. (1977): A numerical approach to testing the fission hypothesis. *Astronom J,* vol. 8, pp. 1013-1024.

Ma, Q. W. (2007): Numerical generation of freak waves using MLPG_R and QALE-FEM methods. *CMES: Computer Modeling in Engineering and Sciences*, vol. 18, No. 3, pp. 223-234.

Ma, Q. W. (2008): A New Meshless Interpolation Scheme for MLPG_RMethod. *CMES: Computer Modeling in Engineering and Sciences*, vol. 23, No. 2, pp. 75-89.

Ma, Q. W.; Yan, S. (2006): Quasi ALE finite element method for nonlinear water waves. *J Comput Phys*, vol. 212, pp. 52-72.

Ma, Q. W.; Zhou, J. T. (2009): MLPG_R method for numerical simulation of 2D breaking waves. *CMES: Computer Modeling in Engineering and Sciences*, vol. 43, No. 3, pp. 277-303.

Mai-Cao, L.; Tran-Cong, T. (2005): A meshless IRBFN-based method for transient problems. *CMES: Computer Modeling in Engineering and Sciences*, vol. 7, No. 2, pp. 149-171.

Mai-Cao, L.; Tran-Cong, T. (2008): A Meshless Approach to Capturing Moving Interfaces in Passive Transport Problems. *CMES: Computer Modeling in Engineering and Sciences*, vol. 31, No. 3, pp. 157-188.

Miller, J. H. (1971): On the Location of Zeros of Certain Classes of Polynomials with Applications to Numerical Analysis. *J Inst Math Appl*, vol. 8, pp. 397-406.

Mulay, S. S.; Li, H. (2009): Analysis of Microelectromechanical Systems Using the Meshless Random Differential Quadrature Method. *Advanced Materials Research*, vol. 74, pp. 29-32.

Mulay, S. S.; Li, H.; See, S. (2009): On the random differential quadrature (RDQ) method: Consistency analysis and application in elasticity problems. *Comput Mech*, vol. 44, pp. 563-590.

Pini, G.; Mazzia, A.; Sartoretto, F. (2008): Accurate MLPG Solution of 3D Potential Problems. *CMES: Computer Modeling in Engineering and Sciences*, vol. 36, No. 1, pp. 43-63.

Quan, J.R.; Chang, C.T. (1989a): New insights in solving distributed system equations by the quadrature method– I. Analysis. *Comput Chem Eng,* vol. 13, pp. 779-788.

Quan, J.R.; Chang, C.T. (1989b): New insights in solving distributed system equations by the quadrature method–II. Numerical experiments. *Comput Chem Eng*, vol. 13, pp. 1017-1024.

Reddy, J. N. (1993): An introduction to the finite element method. McGraw-Hill Inc.

Reutskiy, S. Y. (2008): Meshless Method for Nonlinear, Singular and Generalized Sturm-Liouville Problems. *CMES: Computer Modeling in Engineering and Sciences*, vol. 34, No. 3, pp. 227-252.

Shan, Y. Y.; Shu, C.; Lu, Z. L. (2008): Application of Local MQ-DQ Method to Solve 3D Incompressible Viscous Flows with Curved Boundary. *CMES: Computer Modeling in Engineering and Sciences*, vol. 25, No. 2, pp. 99-113.

Shaw, A.; Banerjee, B.; Roy, D. (2008): A NURBS-based parametric method bridging mesh-free and finite element formulations. *CMES: Computer Modeling in Engineering and Sciences*, vol. 26, No. 1, pp. 31-57.

Shaw, A.; Roy, D. (2007): A novel form of reproducing kernel interpolation method with applications to nonlinear mechanics. *CMES: Computer Modeling in Engineering and Sciences*, vol. 19, No. 1, pp. 69-98.

Shu, C. (2000): Differential Quadrature and its application in Engineering. Springer-Verlag, London.

Shu, C.; Khoo, B. C.; Yeo, K. S. (1994): Numerical solutions of incompressible Navier-Stokes equations by generalized differential quadrature. *Finite Elem Anal Des*, vol. 18, pp. 83-97.

Sigalotti, L. G.; Lopez, H. (2008): Adaptive kernel estimation and SPH tensile instability. *Comput Math Appl,* vol. 55, pp. 23-50.

Sladek, J.; Sladek, V.; Solek, P.; Atluri, S. N. (2008): Modeling of Intelligent Material Systems by the MLPG. *CMES: Computer Modeling in Engineering and Sciences*, vol. 34, No. 3, pp. 273-300.

Sladek, J.; Sladek, V.; Solek, P.; Wen, P. H. (2008): Thermal Bending of Reissner-Mindlin Plates by the MLPG. *CMES: Computer Modeling in Engineering and Sciences*, vol. 28, No. 1, pp. 57-76.

Sladek, J.; Sladek, V.; Tan, C. L.; Atluri, S. N. (2008): Analysis of Transient Heat Conduction in 3D Anisotropic Functionally Graded Solids, by the MLPG Method. *CMES: Computer Modeling in Engineering and Sciences*, vol. 32, No. 3, pp. 161-174.

Sladek, J.; Sladek, V.; Zhang, Ch.; Solek, P. (2007): Application of the MLPG to thermo-piezoelectricity. *CMES: Computer Modeling in Engineering and Sciences*, vol. 22, No. 3, pp. 217-233.

Sladek, J.; Sladek, V.; Zhang, Ch.; Solek, P.; Starek, L. (2007): Fracture analyses in continuously nonhomogeneous piezoelectric solids by the MLPG. *CMES: Computer Modeling in Engineering and Sciences*, vol. 19, No. 3, pp. 247-262.

Strikwerda, J. C. (2004): Finite Difference Schemes and Partial Difference Equations. Society for Industrial and Applied Mathematics.

Swegle, J. W.; Hicks, D. L.; Attaway, S. W. (1995): Smoothed particle Hydrodynamics Stability Analysis. *J Comput Phys,* vol. 116, pp. 123-134.

Tomasiello, S. (2003): Stability and accuracy of the iterative differential quadrature method. *Int J Numer Meth Eng,* vol. 58, pp. 1277-1296.

Wong, S.; Shie, Y. (2008): Large Deformation Analysis with Galerkin based Smoothed Particle Hydrodynamics. *CMES: Computer Modeling in Engineering and Sciences*, vol. 36, No. 2, pp. 97-117.

Wu, C.; Chiu, K.; Wang, Y. (2008): A Differential Reproducing Kernel Particle Method for the Analysis of Multilayered Elastic and Piezoelectric Plates. *CMES: Computer Modeling in Engineering and Sciences*, vol. 27, No. 3, pp. 163-186.

XueHong, W. U.; Shen, S.; Tao, W. (2007): Meshless local Petrov-Galerkin collocation method for two-dimensional heat conduction problems. *CMES: Computer Modeling in Engineering and Sciences*, vol. 22, No. 1, pp. 65-76.

Young, D. L.; Chen K. H.; Lee, C. W. (2005): Novel meshless method for solving the potential problems with arbitrary domain. *J Comput Phys*, vol. 209, pp. 290-321.

Young, D. L.; Chen K. H.; Lee, C. W. (2006): Singular meshless method using double layer potentials for exterior acoustics. *J Acoust Soc Am*, vol. 119, No. 1, pp. 96-107.

Zheng, J.; Long, S.; Xiong, Y.; Li, G. (2009): A Finite Volume Meshless Local Petrov-Galerkin Method for Topology Optimization Design of the Continuum Structures. *CMES: Computer Modeling in Engineering and Sciences*, vol. 42, No. 1, pp. 19-34.

Zong, Z.; Lam, K. Y. (2002): A localized differential quadrature (LDQ) method and its application to 2D wave equation. *Comput Mech*, vol. 29, pp. 382-391

Appendix A: The derivation of characteristic polynomial $\phi(z)$

Following procedure is followed to derive the characteristic polynomial, $\phi(z)$, from the discretized governing PDE. Here, the procedure is explained using the central time and space with multi-step scheme used in Section 3.1.1; similar procedure is followed for rest of the schemes.

From Eq. (16),

$$\left\{a_{j,j-1} \quad a_{j,j} \quad a_{j,j+1}\right\}\begin{Bmatrix}\phi(x_i,t_{j-1})\\ \phi(x_i,t_j)\\ \phi(x_i,t_{j+1})\end{Bmatrix} = a\left\{a_{i,i-1} \quad a_{i,i} \quad a_{i,i+1}\right\}\begin{Bmatrix}\phi(x_{i-1},t_j)\\ \phi(x_i,t_j)\\ \phi(x_{i+1},t_j)\end{Bmatrix} \tag{106}$$

The weighting coefficients from Eq. (106) are computed by Shu's general approach, as given in Eqns. (9) and (10) to give,

$$\phi_m^{j+1} = \phi_m^{j-1} + r\left[-\phi_{m-1}^{j} + \phi_{m+1}^{j}\right] \tag{107}$$

where, $m = i$ and $r = at/h$, where, t and h are the time and space spacings, respectively, as explained in Section 3.2. Taking Fourier inverse on both sides of Eq. (107) gives,

$$\frac{1}{\sqrt{2\pi}}\int_{-\infty}^{+\infty} e^{ihm\xi}\,\hat{\upsilon}^{n+1}(\xi)d\xi = \frac{1}{\sqrt{2\pi}}\int_{-\infty}^{+\infty} e^{ihm\xi}\,\hat{\upsilon}^{n-1}(\xi)d\xi +$$

$$\frac{1}{\sqrt{2\pi}}\int_{-\infty}^{+\infty} r\left(-e^{ih(m-1)\xi}\,\hat{\upsilon}^{n}(\xi)d\xi + e^{ih(m+1)\xi}\,\hat{\upsilon}^{n}(\xi)d\xi\right) \tag{108}$$

where, $n = j$. Rearranging Eq. (108) gives,

$$\frac{1}{\sqrt{2\pi}}\int_{-\infty}^{+\infty} e^{ihm\xi}\left\{\hat{\upsilon}^{n+1}(\xi) - \hat{\upsilon}^{n-1}(\xi) + r\left[e^{-ih\xi} - e^{ih\xi}\right]\hat{\upsilon}^{n}(\xi)\right\}d\xi = 0 \tag{109}$$

to satisfy consistency,

$$\hat{\upsilon}^{n+1}(\xi) - \hat{\upsilon}^{n-1}(\xi) + r\left[\cos(h\xi) - i\sin(h\xi) - \cos(h\xi) - i\sin(h\xi)\right]\hat{\upsilon}^{n}(\xi) = 0 \tag{110}$$

where, $e^{i\theta} = \cos(\theta) + i\sin(\theta)$ relation is used. Substitute $\hat{\upsilon}^{n}(\xi) = \phi^{n}(z)$ and $h\xi = \theta$ in Eq. (110) to get,

$$\phi(z) = z^2 - (2ri\sin\theta)z - 1 \text{ by taking out } \phi^{n-1}(z) \text{ as common} \tag{111}$$

Eq. (111) is same as Eq. (17). Similar procedure is followed to get all the characteristic polynomials referred in this paper.

Appendix B: Definition of reduced polynomial $\phi_1(z)$

If $\phi(z)$ is any general nonzero polynomial of degree n, as given in Eq. (18), and $\phi^*(z)$ is its complex conjugate, as given in Eq. (20), then the reduced polynomial, $\phi_1(z)$, of at most the degree $n-1$ can be defined as,

$$\phi_1(z) = \frac{\phi_0^*(0)\phi(z) - \phi(0)\phi_0^*(z)}{z} \tag{112}$$

The reduced polynomial gives immediate criterion for the self inversiveness of $\phi(z)$ such that $\phi(z)$ is self inversive if and only if $\phi_1(z) = 0$. Its proof can be referred in Miller (1971).

Appendix C: Discretization equation derivation by Taylor series

In this appendix, the discretization equation derivation by Taylor series is explained using Scheme 1 given in Section 3.1.1. Identical procedure is followed in the paper to obtain the rest of the discretization equations.

From Eq. (16),

$$\Rightarrow \left\{a_{j,j-1} \quad a_{j,j} \quad a_{j,j+1}\right\} \begin{Bmatrix} \phi(x_i,t_{j-1}) \\ \phi(x_i,t_j) \\ \phi(x_i,t_{j+1}) \end{Bmatrix} = a\left\{a_{i,i-1} \quad a_{i,i} \quad a_{i,i+1}\right\} \begin{Bmatrix} \phi(x_{i-1},t_j) \\ \phi(x_i,t_j) \\ \phi(x_{i+1},t_j) \end{Bmatrix} \tag{113}$$

The weighting coefficients, $a_{i,j}$, are computed by Shu's general approach using Eqns. (9) and (10) to give,

$$a_{m,m-1} = \frac{-1}{2h}, \quad a_{m,m+1} = \frac{1}{2h}, \quad a_{m,m} = 0 \tag{114}$$

and

$$a_{n,n-1} = \frac{-1}{2t}, \quad a_{n,n+1} = \frac{1}{2t}, \quad a_{n,n} = 0 \tag{115}$$

where, $m = j$ and $n = i$. Substituting Eqns. (114) and (115) into Eq. (113) lead to,

$$\phi_m^{n+1} = \phi_m^{n-1} + r\left[-\phi_{m-1}^n + \phi_{m+1}^n\right] \tag{116}$$

The ϕ terms from Eq. (116) are replaced by Taylor series expansion as,

$$\phi_{m-1}^n = \phi(x_m - h) = \phi - h\phi_{,x} + \frac{h^2}{2}\phi_{,xx} - o(h)^3 \tag{117}$$

$$\phi_{m+1}^{n} = \phi(x_m + h) = \phi + h\phi_{,x} + \frac{h^2}{2}\phi_{,xx} + o(h)^3 \tag{118}$$

$$\phi_{m}^{n-1} = \phi(t_n - t) = \phi - t\phi_{,t} + \frac{t^2}{2}\phi_{,tt} - o(t)^3 \tag{119}$$

$$\phi_{m}^{n+1} = \phi(t_n + t) = \phi + t\phi_{,t} + \frac{t^2}{2}\phi_{,tt} + o(t)^3 \tag{120}$$

where, $\phi = \phi_m^n$. Substituting Eqns. (117) to (120) in Eq. (116) and simplifying,

$$\phi_{,t} - a\phi_{,x} = \phi_{,xxx}\left[\frac{ah^2}{6} - \frac{t^2a^3}{6}\right] \tag{121}$$

where, $\phi_{,ttt} = a^3\phi_{,xxx}$. Thus, Eq. (121) is same as Eq. (49).